CHAPTER 4

RESULTS AND DISCUSSION

Part I Acquisition of bioactive compounds from TD plant

Firstly, TD was identified in accordance with four typical characteristics including evergreen shrub forms shaped like symmetrical mounds 6-feet high, horizontal branches having the appearance of an attractive, almost horizontal shrub (the species name, *divaricata*, means an obtuse angle), large, shiny, deep green leaves, 6 or more inches in length and 2 inches wide and waxy blossoms with white, five-petal pinwheels, gathered in small clusters on the stem tips. The voucher specimen collection of TD used in the present study was kept in the herbarium of Faculty of Pharmacy, Chiang Mai University, Thailand. Then the stems of the identified TD were selected for the further experiments. Taesotikul *et al*. (1989) showed the resemble yield of both ethanolic extracts from root and stem part of TD (64) while Ingkaninan *et al*. (2006) has revealed that both extracts exhibited very high inhibitory activity (>90%) against AChE at the concentration of 0.1 mg/mL in ethanol (5). Since the reproducibility of the stem as well as the abundant amount when compared with the root, the stem part of TD was selected for the present study. The maceration of dried TD stem in 95% ethanol gave a TD crude extract which was brown-green sticky semisolid (**Figure 8a**). The TD crude extract was further purified by acid-base extraction to give the TD alkaloidal extract which was brown solid (**Figure 8b**). The yields of both extracts are shown in **table 5**.

(a) (b)

Figure 8 TD crude extract (a) and TD alkaloidal extract (b).

Table 5 % Yield of TD crude extract and TD alkaloidal extract.

Materials	% Yield
TD crude extract	3.67
TD alkaloidal extract	0.82

Nowadays, the construction of chromatographic fingerprints of complex herbal extract has become one of the most powerful approaches to conduct quality control because of its simplicity and reliability (65). TLC is the common method of choice for herbal analysis and frequently used since the advantages of using TLC include its simplicity, versatility, high velocity, specific sensitivity and simple sample preparation (66). Therefore, TLC fingerprints of TD alkaloidal extract was constructed to be a tool for identification, authentication and quality control. There are many ways to detect the TLC including physical, chemical, and enzymatic and biological detection methods.

The physical detection which based on the absorption of electromagnetic radiation (often UV or visible light) is the most common method. Coloured substances are directly visible using light in the visible range. However, the TLC chromatogram of TD alkaloidal extract showed nothing in daylight since the compositions of TD alkaloidal extract were colorless. Therefore, the TLC chromatogram was then inspected under UV-light, short wavelength (254 nm) and long wavelength (365 nm). The TLC plate of silica gel GF-254 (2 cm × 6 cm) was used to observe the fluorescence quenching. Under the short wavelength UV light, the plate was seen as a bright fluorescent sheet and the solutes were observed as dark non-fluorescent spots where the solutes have quenched the plate fluorescence as shown in **Figure 9a**. The Rf values of prominent spots observed were 0.31, 0.49, and 0.67, respectively. Among these spots, the spot at the Rf value of 0.67 is the major constituents because of their highest intensity. Some compounds show auto-fluorescence after irradiation with long wavelength UV light from a high-pressure mercury vapour lamp as shown in **Figure 9b**. The Rf values of prominent fluorescence spots observed under UV at 366 nm were 0.43, 0.51, 0.57, 0.62, 0.85 and 0.92, respectively.

The chemical detection method is base on colour reactions which have been used for quite a long time in qualitative analysis. Such colour reactions can be used very conveniently with TLC, simply by spraying the plates with the colouring reagents. Dragendorff's reagent is used to identify the alkaloids in this study. After that the TLC plate was developed, it was sprayed with Dragendorff's reagent and inspected in daylight to visualize the alkaloids. The positive result referring to alkaloid was observed as oranges spots on the yellow background. The alkaloids were

found at the Rf values of 0.49 and 0.67 as shown in **Figure 9c**. Therefore, the major constituents of TD alkaloidal extract (Rf value = 0.67) are alkaloids.

The enzymatic and biological detection method as previously described in the study of Rhee, *et al*. (2001) was used to reveal the anti-ChE of the components in TD alkaloidal extract (56). After another TLC plate was developed, it was then stained using Ellman's reagent to detect anti-ChE. The results as shown in **Figure 9d** indicated that the alkaloids with Rf value of 0.67 which is the major constituents of TD alkaloidal extract posses AChE inhibitory activity.

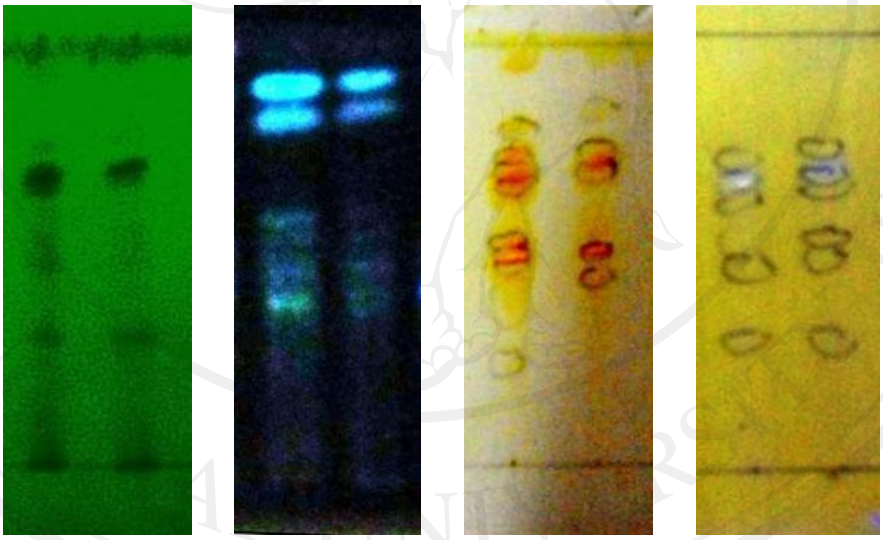

(a) (b) (c) (d)

Figure 9 TLC chromatogram of TD alkaloidal extract viewed under UV at 254 nm (a), UV at 366 nm (b), after sprayed with dragendorff's reagent (c) and after sprayed with Ellman's reagent (d) when the mobile phase was dichloromethane: methanol = 9:1.

Qualitative analysis is typically used to demonstrate the general characteristics of plant extract with regard to quality consistency and stability. HPLC is a popular method for quality control of plant extract because it is accurate, precise and not limited by the volatility or stability of the sample compounds (66). It is necessary to notice that the optimal separation condition for the HPLC involves many factors, therefore, a good experimental design for the optimal separation seems in general necessary (67). A reversed phase column Inertsil® ODS-2 (250 × 4.6 mm i.d., 5 µm, GL Sciences Inc., Japan) connected with a guard column (125 × 4.6 mm i.d., 5 µm, Algilent, USA) was used for the proposes of quality and quantity analyses. The most common problem in reversed phase HPLC analysis of alkaloids is tailing and peak broadening due to the interaction of the basic nitrogens of the alkaloids and residual acidic silanol groups on the stationary phases, therefore, the addition of tertiary or quaternary amines to the mobile phase is adopted to avoid these problems (68). Consequently, ammonia solution was employed to adjust the pH of PBS used in the mobile phase when the mobile phase composed of methanol and PBS (pH 7.4) in the ratio of 86:14. The HPLC chromatogram of 20 µL injected sample (1 mg/mL) which detected at 295 nm is shown in **Figure 10**. There were 4 major peaks which were found at the retention time of 8.298, 10.744, 12.178 and 15.642 min, respectively. The peak at the retention time of 12.178 min was found as the most prominent peak with AUC of 11.832±0.027%. The qualitative identification can be made using these retention data and percentage of AUC.

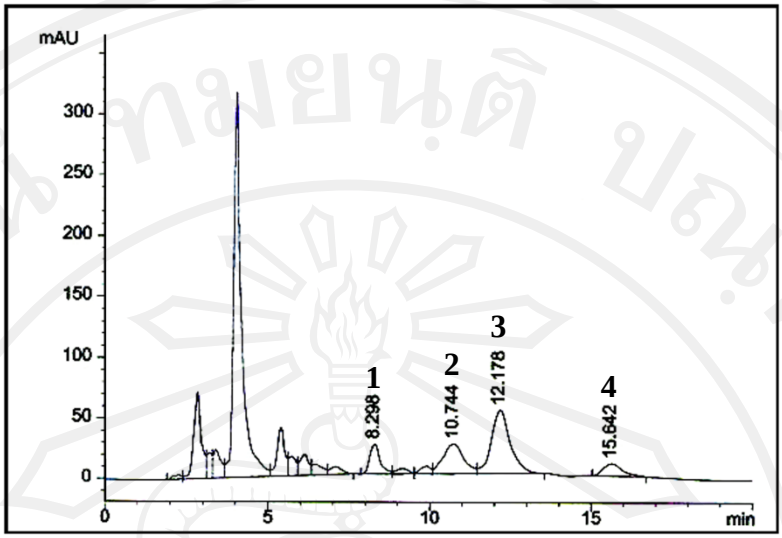

Figure 10 HPLC chromatogram of TD alkaloidal extract when the stationary phase was reversed phase column Inertsil® ODS-2 and mobile phase was a mixture of methanol and phosphate buffer (pH 7.4) in the ratio of 86:14.

In order to determine the amount of an active component present in TD alkaloidal extract using the HPLC technique, reference material or marker that serves as an external standard is required. As can be seen in **Figure 10**, the major peak at the retention time of 12.178 min would be the standard of choice for the quantitative analysis. Since there is no pure alkaloid commercially available, every laboratory willing to perform this analysis would first need to isolate and characterize the pure substance (69). Therefore, the marker of TD alkaloidal extract needs to be separated and identified. Sephadex, cross-linked dextran gel, was selected for separating the pure marker because of its reusable. Gel filtration chromatography separates the compounds on the basis of size (70). When molecules move through a bed of porous beads, they diffuse into the beads to greater or lesser degrees. Smaller molecules

diffuse further into the pores of the beads and therefore move through the bed more slowly, while larger molecules enter less or not at all and thus move through the bed more quickly. Therefore, both molecular weight and three-dimensional shape contribute to the degree of retention (70). Methanol was used as an eluent to elute the compounds of TD alkaloidal extract throughout the Sephadex column.

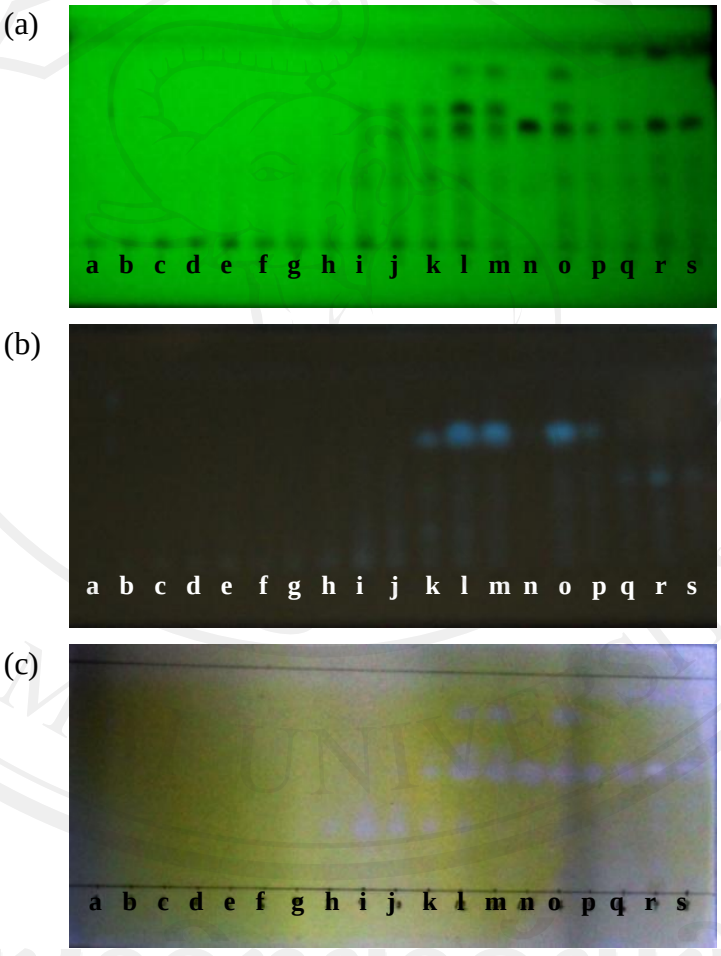

Figure 11 TLC chromatogram of fractions collected from Sephadex column of TD alkaloidal extract inspected under UV at 254 nm (a), UV at 366 nm (b) and after sprayed with Ellman's reagent (c) when the mobile phase was dichloromethane: methanol = 9:1.

"Fraction n" as shown in **Figure 11** supposed to be a pure compound since it had only one spot in the TLC chromatogram inspected under UV of 254 nm and no impurity under UV of 366 nm. Two different developing solvent systems, dichloromethane : methanol = 9:1 and diethylether : dichloromethane : methanol = 8:1.5:0.5, were used to confirm the purity of this fraction. The TLC combined with enzymatic and biological detection indicated the anticholinesterase activity of "fraction n" because of the white spot observed on the yellow background. Therefore, the pure compound of this fraction might be the biological marker for the TD alkaloidal extract. Although the results from TLC chromatogram indicated the purity of "fraction n", it needed to be confirmed by more method including HPLC. The HPLC chromatogram of "fraction n" as shown in **Figure 12** could confirm the purity of this fraction since there was only one peak observed at the retention time of 12.325 min which was the same retention time as the most prominent peak in TD alkaloidal extract. Therefore, "fraction n" would be an appropriate marker for quantitative determination.

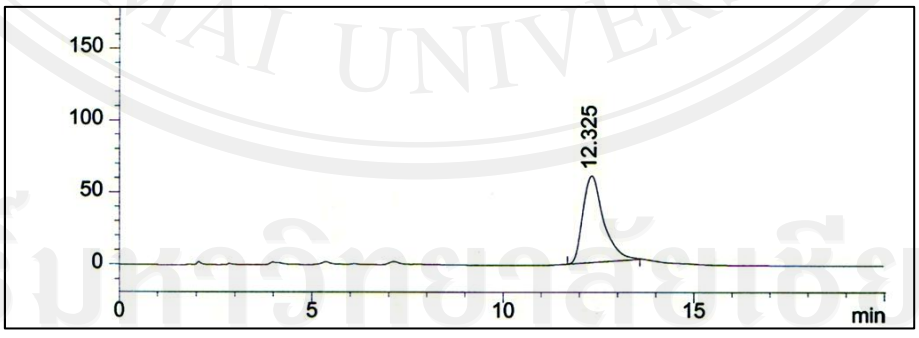

Figure 12 HPLC chromatogram of pure alkaloid when the stationary phase was reversed phase column Inertsil® ODS-2 and mobile phase was a mixture of methanol and PBS (pH 7.4) in the ratio of 86:14.

The spectrum index screen by photodiode array (PDA) detector was used to confirm the peak purity of pure alkaloid. This method used spectra at three sampling points on the peak include upslope point, peak top and downslope point. All three points showed the same spectra as shown in **Figure 13**, indicating the maximum absorbance at 223, 285 and 295 nm.

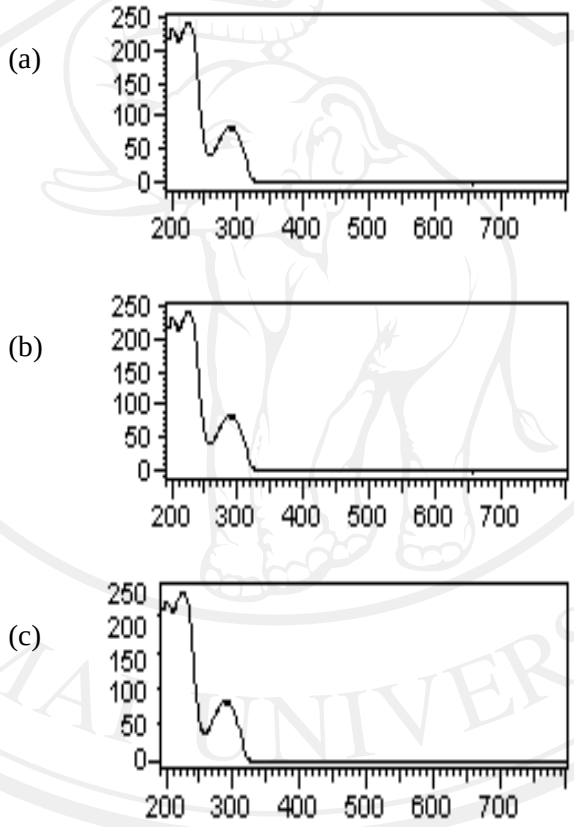

Figure 13 Spectra at upslope point (a), peak top (b) and downslope point (c) of pure alkaloid detected by PDA when the stationary phase was reversed phase column Inertsil® ODS-2 and mobile phase was a mixture of methanol and PBS (pH 7.4) in the ratio of 86:14.

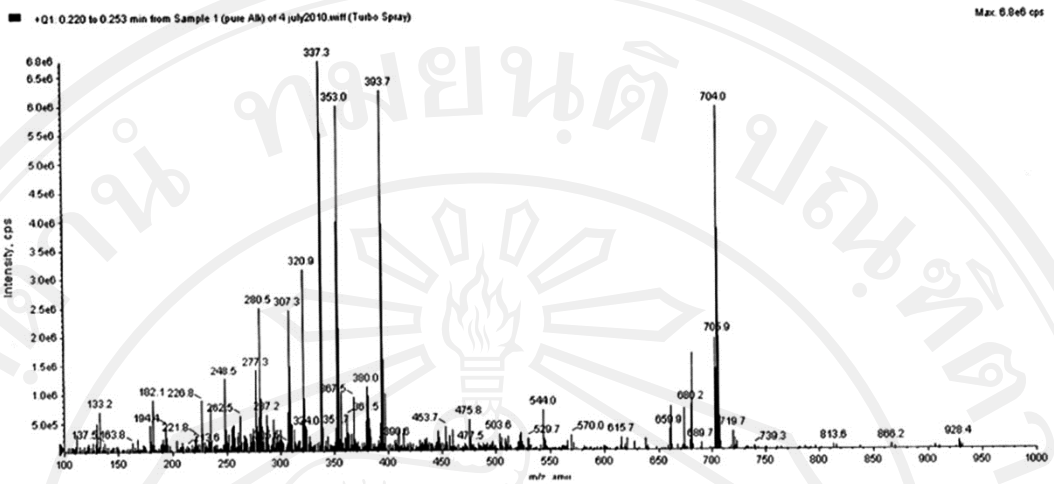

Figure 14 Mass spectral of 3'-*R/S*-hydroxyvoacamine isolated from TD stem.

The negative mode MS of 3'-*R/S*-hydroxyvoacamine as shown in **Figure 14** displays a peak at *m/z* 719 $[M-H]^-$ suggesting the molecular formula of $C_{43}H_{52}N_4O_6$. The major peak at *m/z* 704 probably corresponded with $[M-OH]^-$. Moreover, a peak at *m/z* 337 corresponded well with the vobasinyl moiety ($C_{21}H_{25}N_2O_2$). ^{1}H-NMR and ^{13}C-NMR spectra suggested that 3'-*R/S*-hydroxyvoacamine was vobasinyl-iboga type bisindole alkaloid. The spectral data of 3'-*R/S*-hydroxyvoacamine is shown in **Table 6**. It should be noted that several duplicate signals were observed in the ^{1}H-NMR spectrum showing the presence of 3'-*R/S* stereoisomeric forms of the indole alkaloid. Six aromatic protons provided a clue concerning the constitution of two indole rings with the substitutions. The results from HMQC indicated that the complex proton signals at δ 7.06 which the integrals were 3 directly bonded with three carbon atoms (C-10, C-11 and C-12). Therefore, it was assigned to be H10, H11 and H12, respectively. The duplications can be seen in the aromatic signals at δ 6.94/6.93 from H9 and 6.77/6.75 from H12. The broad singlets at δ 7.49 and δ 7.69 were assigned to the amine hydrogens of the indole rings. Moreover, the ^{1}H-NMR spectrum exhibited

two singlet methyl signals for two carbomethoxy groups at δ 2.46 and 3.63. The results from HMBC revealed that the first carbomethoxy group is attached to C-16' of a vobasinyl moiety and the second group attached to C-16 of an iboga moiety. One aromatic methoxy group and one N-methyl group were revealed at δ 4.00 (board singlet with 3H) and δ 2.58 (singlet with 3H), respectively. A double bond between C19 and C20 was revealed since the chemical shift of C19 was as high as 118.52 ppm and directly bonded with a proton, showing the signal at δ 5.31. The NMR spectra of 3'-*R/S*-hydroxyvoacamine were very similar to those of voacamine, except for the signal of C3' where a hydroxyl group is attached (71). The duplication was also found at this position. The chemical shift of C3' was as high as 96.00/86.19 which referred to the substitution of a hydroxyl group. With all these evidences, the structure was thus identified as 3'-*R/S*-hydroxyvoacamine.

The chemical structure of 3'-*R/S*-hydroxyvoacamine is shown in **Figure 15**. Normally, the 3'-hydroxy derivatives of voacamine occurred as a mixture of the 3'*R* and 3'*S* isomers. Therefore, duplication can be seen in some proton and carbon signals (**Table 6**). The occurrence of 3'*R* and 3'*S* mixtures of 3'-hydroxyiboga alkaloids has been reported in the literatures of several species of *Tabernaemontana* (72-74). In previous studies, 3'-*R/S*-hydroxyvoacamine has been isolated from the root bark of *T. chippii* (75) and the stem bark of *T. dichotoma* (76). However, ^{13}C-NMR data of 3'-*R/S*-hydroxyvoacamine have not been reported before. Our study is the first one to present the complete assignment of the NMR spectra of this compound.

Table 6 ^{13}C and ^{1}H NMR spectral data of 3'-*R/S*-hydroxyvoacamine.

No.	δ_C		δ_H (*J*/Hz)		HMBC
	3'*R*	**3'*S***	**3'*R***	**3'*S***	
2	137.02	135.59			H-6, H-21
3	96.00	86.19	3.91 s	4.32 s	H-21
5	52.55	51.24			H-21
6	21.98	21.91	3.03 dd (7.8;5.8)	3.03 dd (7.8;5.8)	
7	109.66	109.66			H-6
8	130.14	130.14			H-9
9	99.06	99.06	6.94 s	6.93 s	
10	151.00	151.00			H-9
11	130.24	130.24			H-9
12	110.45	110.45	6.77 s	6.75 s	
13	130.36	130.36			H-9
14	34.44	29.95	1.96 m	1.80 m	
15	24.96	24.66	1.68-1.25 m		H-21
16	54.05	54.23			H-21
17	35.44	35.35	2.61 m, 1.82 (14) b	2.61 m	H-21
18	11.64	11.64	0.90 t	0.88 t	
19	26.63	26.90	1.4-1.6 m	1.4-1.6 m	H-21
20	37.69	37.61	1.40 m	1.40 m	H-21, H-18
21	55.33	56.10	3.76 s	3.72 s	
COOMe	52.49	52.49	3.63 s [3H]	3.63 s [3H]	
COOMe	174.46	174.46			COOMe, H-21
OMe	55.99	55.99	4.00 sbr [3H]	4.00 sbr [3H]	H-21, H-18
-NH			7.69 sbr	7.69 sbr	
2'	138.09				H-6'
3'	36.30		5.13 dbr		
5'	59.92		4.00 m		NMe, H-16', H-21', H-6'
6'	19.43		3.48 m, 3.23 m		H-16'
7'	110.45				H-6'
8'	129.84				H-10', H-12'
9'	117.43		7.54 m		H-11'
10'	118.89		7.06 m		H-9'
11'	121.53		7.06 m		H-9'
12'	109.81		7.06 m		H-9'
13'	135.81				H-9', H-11'
14'	37.20		1.94 m		
15'	33.60		3.73 m		
16'	47.05		2.71 dd		
18'	12.25		1.66 d (6.8) [3H]		H-19'
19'	118.52		5.31 q (6.7)		H-18', H-21'
20'	138.09				H-18' H-16', H-21'
21'	52.49		3.80-3.58 m, 2.89 d (13.7)		
COOMe	49.89		2.46 s [3H]		
COOMe	171.67				H-16',COOMe
NMe	42.44		2.58 s [3H]		
-NH			7.49 sbr		

s, singlet; d, doublet; t, triplet; m, mutiplet; dd, doublet of doublet; dt, doublet of triplet; br d, board doublet; *J*, 1H–1H coupling constants.

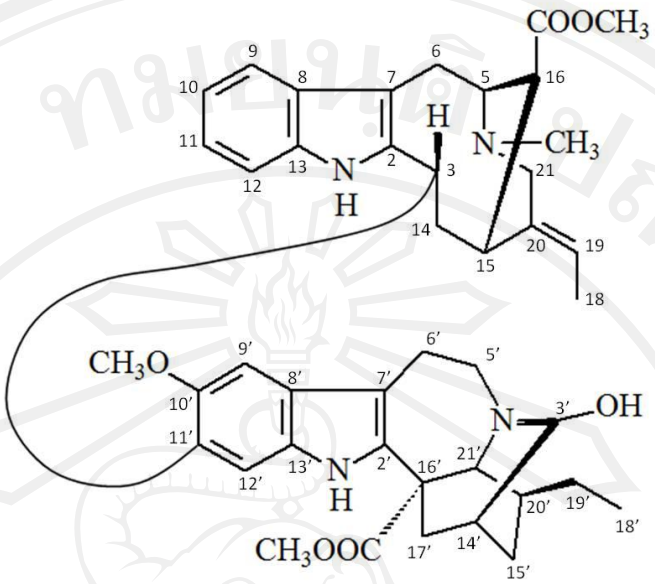

Figure 15 Structure of 3'-*R/S*-hydroxyvoacamine isolated from TD stem.

Moreover, the exhaustive investigation in cholinesterase inhibitory activity of 3'-*R/S*-hydroxyvoacamine was investigated. The inhibitory activity against AChE is shown as a dose response curve in **Figure 16**. The IC_{50} value calculated from the graphpad/prism program was 6.996±1.993 µM. Enzyme kinetic which is a function of the concentration of substrate available to the enzyme is illustrated in **Figure 17.** The relationship between the initial rate of a reaction (V) and the substrate concentration ([S]) has been described by Michaelis-Menten equation; $V = V_{max}$ [S] / ($K_m + V_{max}$), where V_{max} is the maximal velocity or rate of a reaction at saturating substrate concentrations and K_m is the substrate concentration when the velocity of the reaction reaches one-half of V_{max}. As the concentration of ATCI which was a substrate in the reaction increased, the increase in the rate of the reaction was reduced since the enzyme eventually approached saturation. At the saturation stage, increasing the substrate concentration did not change the rate of the reaction because all enzymes

were engaged in catalysis. On the other hand, the data were plotted according to Lineweaver-Burk equation; $1/V = \{(K_m/V_{max}) \times 1/[S]\} + 1/V_{max}$. In contrast to the Michaelis-Menten equation which demonstrated the hyperbolic plot, the Lineweaver-Burk plot is linear as shown in **Figure 18.** The values of V_{max} and K_m can be determined by extrapolating the line to intercept both axis of Y and X. The intercept on the Y-axis represents $1/V_{max}$ whereas the intercept on the X-axis represents $-1/K_m$. The V_{max} and K_m values of a human AChE-catalyzed reaction and the reaction in the presence of a pure alkaloid were shown in **Table 7**. The difference in V_{max} values and the similarity in K_m values indicated that it acted as a noncompetitive inhibitor. As K_m is a parameter indicating the affinity of enzyme with the substrates, the unchanged of K_m value when the pure alkaloid was presented, showed that the pure alkaloid bound to a region other than the active site of AChE. This alkaloid inhibited AChE in the same fashion as other AD drugs including donepezil, tacrine and rivastigmine which are noncompetitive inhibitor (77).

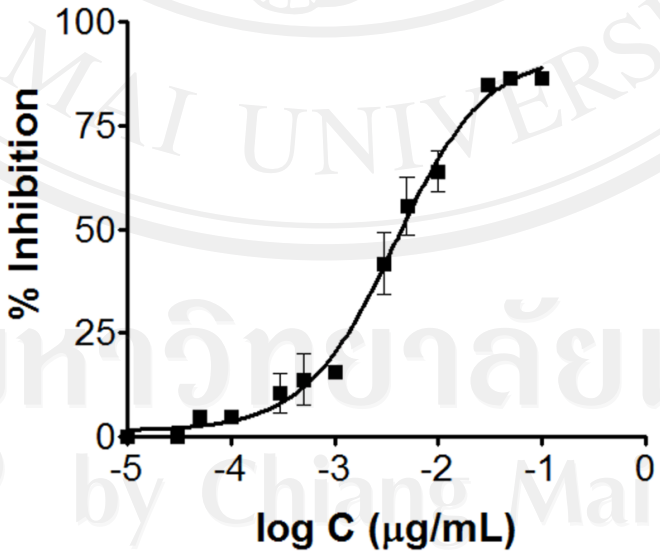

Figure 16 Dose response curve of 3'-*R/S*-hydroxyvoacamine against AChE.

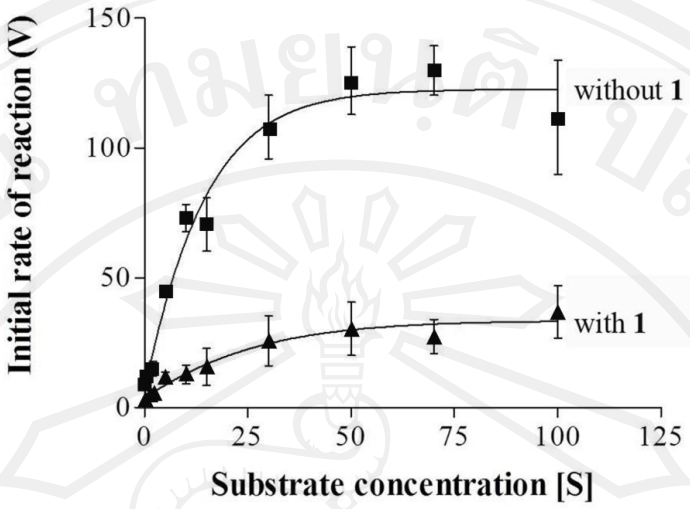

Figure 17 The rate of reaction (*V*) plotted against substrate concentration ([*S*]) for a human AChE-catalyzed reaction (■) and the reaction in the presence of 3'-*R/S*-hydroxyvoacamine (▲).

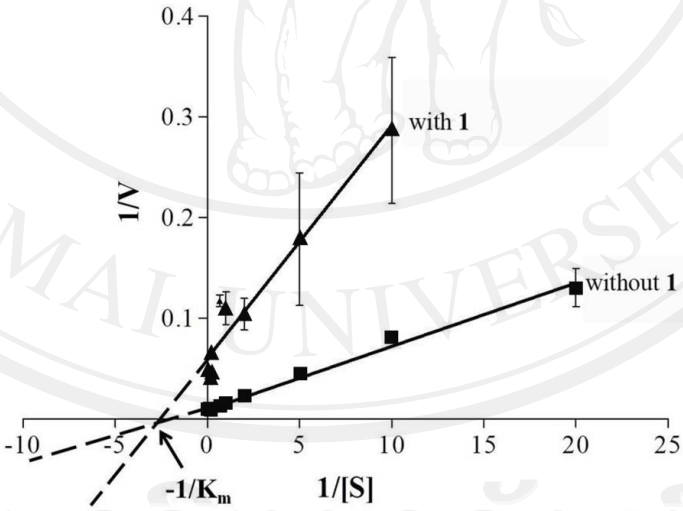

Figure 18 Lineweaver-Burk plot of the inverse rate of reaction (1/*V*) against the inverse substrate concentration (1/[*S*]) for a human AChE-catalyzed reaction (■) and the reaction in the presence of a pure alkaloid (▲). The values are plotted and extrapolated (dashed line) to intercept the X- axe. The X-axis intercept is equal to -1/K_m, and the Y-axis intercept is equal to 1/V_{max}.

Table 7 V_{max} and K_m values of a human AChE-catalyzed reaction and the reaction in the presence of 3'-*R/S*-hydroxyvoacamine.

Parameters	Human AChE-catalyzed reaction	
	Without 3'-*R/S*-hydroxyvoacamine	**With 3'-*R/S*-hydroxyvoacamine**
V_{max}	157.1	44.27
K_m	1433	1586

The HPLC method was validated according to the ICH guidelines (78). LOD and LOQ of 3'-*R/S*-hydroxyvoacamine were investigated using the S/N ratio of the chromatogram. The concentration that purified alkaloid solution showed the S/N ratio of 3:1 was established as LOD, whereas, the S/N ratio of 10:1 was established as LOQ. When the injection volume was 20 µL, S/N ratio of 3:1 was detected at the 0.75 µg/mL which was equivalent to 0.015 µg of the pure alkaloid. In addition, S/N ratio of 10:1 detected at the 2.5 µg/mL was equivalent to 0.050 µg of the pure compound. Therefore, LOD and LOQ of this pure alkaloid were 0.015 and 0.050 µg, respectively.

The calibration curve of purified alkaloid was established when the smallest amount of the pure alkaloid was LOD amount. Slope and intercept of the calibration curve were 755.91 and -0.0969, respectively. The correlation coefficient was 0.9999 indicated the linear range as shown in **Figure 19**.

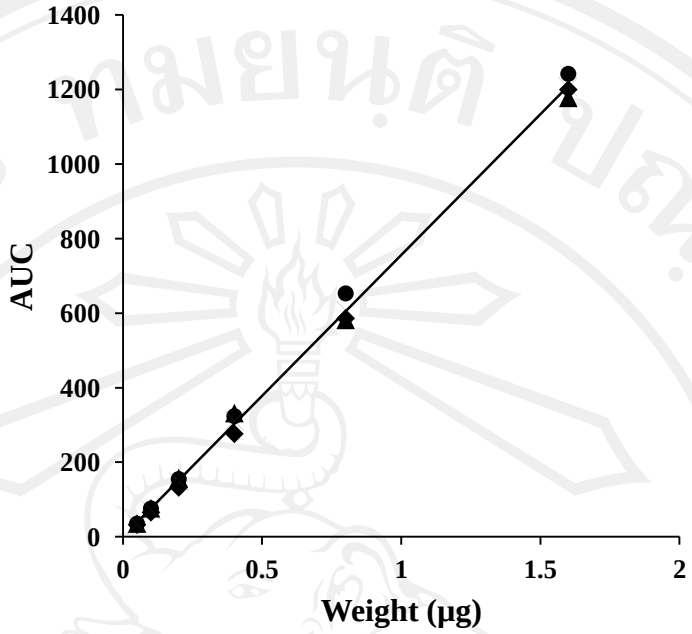

Figure 19 Calibration curve of the pure alkaloid from HPLC analysis (n = 3).

The precision of an analytical procedure expresses the closeness of agreement (degree of scatter) between a series of measurements obtained from multiple sampling of the same homogeneous sample under the prescribed conditions (78). Repeatability or intraday precision expresses the precision under the same operating conditions over a short interval of time. Mean, S.D. and relative standard deviation (% R.S.D.) for every concentration level were calculated and shown in **Table 8**. All the repeatability was in acceptance criteria although smaller concentration tends to have higher variation. The intermediate precision which expresses within-laboratories variations were also in the acceptance criteria.

Table 8 Precision on different days and different concentration levels.

	Mean	S.D.	% R.S.D.
Repeatability (n = 6)			
80 mg/mL	1177.78	0.60	0.05
40 mg/mL	653.11	0.23	0.04
20 mg/mL	332.27	0.39	0.12
10 mg/mL	157.77	0.55	0.35
5 mg/mL	76.79	0.17	0.22
2.5 mg/mL	35.79	0.21	0.58
Intermediate precision (3 days, n=6)			
80 mg/mL	1206.56	32.68	2.71
2.5 mg/mL	34.64	1.73	5.00

The accuracy of an analytical procedure expresses the closeness of agreement between the value which is accepted either as a conventional true value or an accepted reference value and the value found (78). The mean recovery and S.D. were calculated. A mean recovery of 99.42% with S.D. of 0.20 was obtained. Based on these results the recovery was considered to be acceptable.

<u>Part II</u> Anticholinesterase activity determination

AD, a neurodegenerative disorder, affects an estimated number of more than 18 million elderly people worldwide. This disease is associated with intellectual malfunction and subsequent decline in cognitive, behavioral and motor functions (79-80). Increased levels of AChE have been found in post-mortem brain samples of AD patients which have led to the hypothesis that the cognitive decline in AD patients is related to progressive cholinergic degeneration (81). Since choline is a neurotransmitter released at the synaptic gap. The pathological features in central nervous system disorders are identified by neurotransmitter disturbances and insufficient especially in cholinergic functions (82). Normally, choline is hydrolyzed by cholinesterase enzyme. Greater amount of the enzyme lead to lower amount of choline found in the synaptic gap. Inhibition of cholinesterase therefore can restore the level of the choline in the brain (83). Nowadays, enhancing ACh levels in the brain using AChEIs to suppress the ACh degradation is one of the most promising approaches for treating AD (5, 84-89). There are a few synthetic medicines, e.g. tacrine, donepezil, and the natural product-based rivastigmine and galantamine for treatment of cognitive dysfunction and memory loss associated with AD (6, 7, 87-88). Nevertheless, none of them can cease the disease. Consequently, there is still a great demand for new drug candidates for AD treatment. Particularly, natural sources might be used to isolate such compounds. The extract from TD has been reported to possess anticholinesterase activity (5, 9, 10, 29). However, the anti-ChE of TD alkaloidal extract has not been studied before. Therefore, the present study aims to investigate the anti-ChE of TD alkaloidal extract for the further pharmaceutical proposes.

The dose response curves of TD alkaloidal extract in a comparison with galantamine, a well-known cholinesterase inhibitor in the market, against AChE and BChE were shown in **Figure 20** and the IC_{50} values calculated from the graphpad/prism program were shown in **Table 9**. TD alkaloidal extract exhibited as high potential as galantamine in AChE inhibition. The AChE inhibition of TD alkaloidal extract was not different from the standard galantamine ($p < 0.01$) while the BChE inhibition was much less than that of galantamine. These results can indicate the selectivity of TD alkaloidal extract on AChE inhibition.

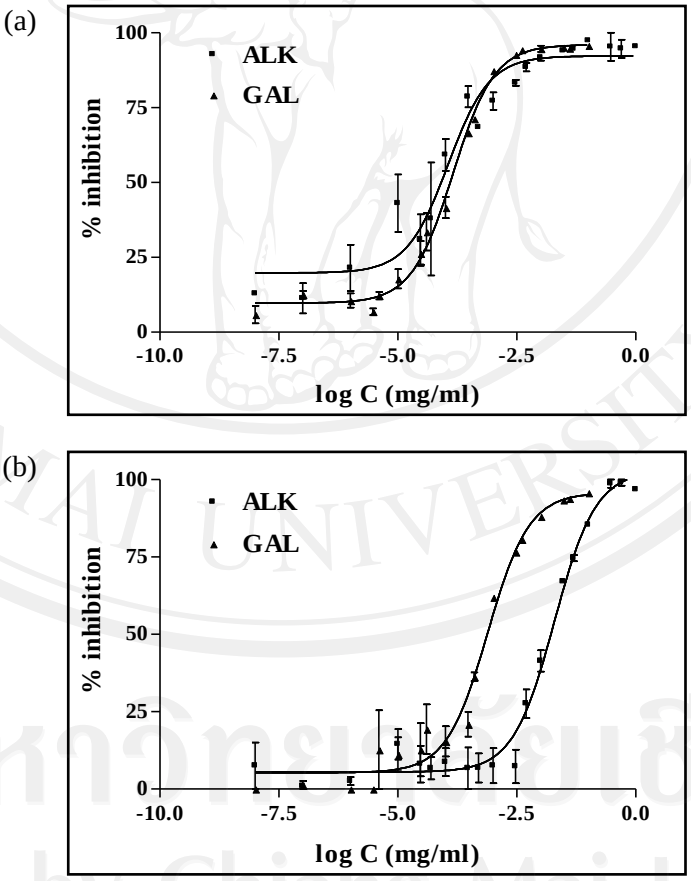

Figure 20 Dose response curve of TD alkaloidal extract (■) compared with galantamine (▲) against AChE (a) and BChE (b).

Table 9 IC_{50} values of TD alkaloidal extract compared with galantamine against AChE and BChE.

IC_{50} (ng/mL)	TD alkaloidal extract		Galantamine	
	AChE	**BChE**	**AChE**	**BChE**
1.	142.7	19150	162.7	797.4
2.	142.8	22850	130.5	657.3
3.	108.0	17460	139.7	895.4
mean	**131.17**	**19820.00**	**144.30**	**783.37**
S.D.	**20.06**	**2756.76**	**16.59**	**119.67**

The MWM test was employed to evaluate the maintenance in learning ability of the amnesia induced mice after receiving TD alkaloidal extract. In this procedure, the mice did not need to be deprived of food to motivate learning and the use of electric shock to motivate escape behaviour is obviated because mice are natural swimmers and take to water-escape tasks easily (58). In the experiments, the mice were placed into a circular pool of water from which they can escape onto a hidden platform. The platform was hidden beneath the opaque water to avoid the local cues to guide escape behaviour. Escape latency, the time that each mouse used for finding out the hidden platform, was used as a quantitative measurement. **Figure 21** shows the escape latency of the control group which receive no treatment throughout the study. The learning ability of the normal mice by MWM can be seen. The shorter escape latency in the later days provided evidence that the mice escape by learning the spatial position of the platform.

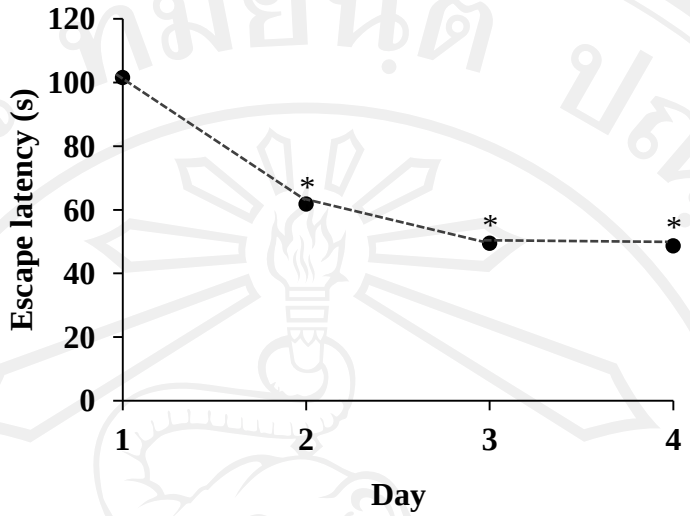

Figure 21 Escape latency of control group (n = 11) in the training phase ($p < 0.05$).

There are several methods to induce the amnesia condition in mice such as scopolamine (muscarinic antagonist) injection (89), centrally administered Aβ (90), MK-801 (an NMDA receptor antagonist) injection (91), N_{ω}-nitro-$_L$-arginine (L-NNA) (a nitric oxide inhibitor) injection (91), etc. However, scopolamine was used as a standard drug for inducing cognitive deficits in mice in the present study because scopolamine-induced amnesia was most likely caused by a blockage of cholinergic signalling. Scopolamine has been used in cognitive deficits animal model associated with Alzheimer's dementia and became very popular after the cholinergic hypothesis of geriatric memory dysfunction was postulated (89). Recall of platform position was assessed by a probe test, at 1 and 3 days following the training phase, in which the platform was removed and the mice were allowed to freely swim and explore the maze for 60 s. The time that each mouse spent in the quadrant where the platform had been located was used as a tool for repeated measurements of spatial memory. The

significant less time in the target quadrant of the mice with scopolamine injections can indicate the scopolamine induced amnesia condition of them (**Figure 22**).

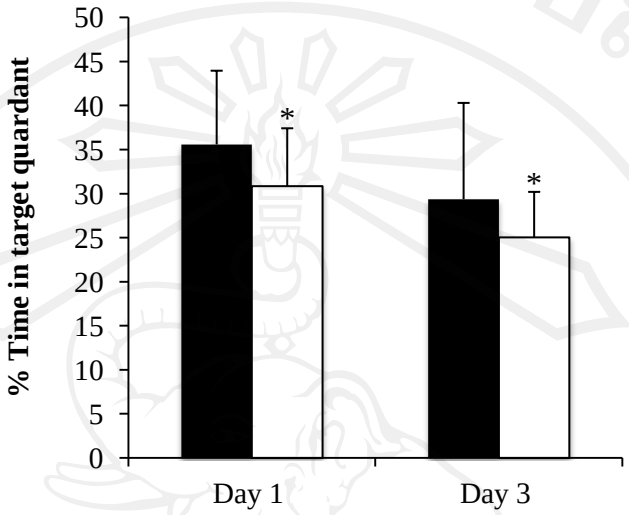

Figure 22 Time in target quadrant of control group (■) and scopolamine group (□) in probe test (n = 6, $p < 0.05$).

The influence of transdermal TD alkaloidal extract on the recall of the spatial learning task was determined using a probe test on days 1 and 3 following the training session. TD alkaloidal extract dissolved in PG at the dose of 250, 500 or 1,000 mg/kg was applied via transdermal route on the back-shaved mice, whereas galantamine, a positive cholinesterase inhibitor, was delivered via oral route. Although the routes of administration were different, the aim of both administration routes was to enter the systemic system and pass through the brain. Since there has not been any model using transdermal anti-ChE drug as a positive control before, the orally galantamine was selected for this study. Over the two recall sessions, the mice treated with TD alkaloidal extract (1,000 and 500 mg/kg) and galantamine spent significantly more time searching in the target quadrant on days 1 and 3 as compared to the scopolamine

induced amnesia mice (**Figure 23**). This can indicate the same potential in cognitive enhancing properties of transdermal TD alkaloidal extract as oral galantamine.

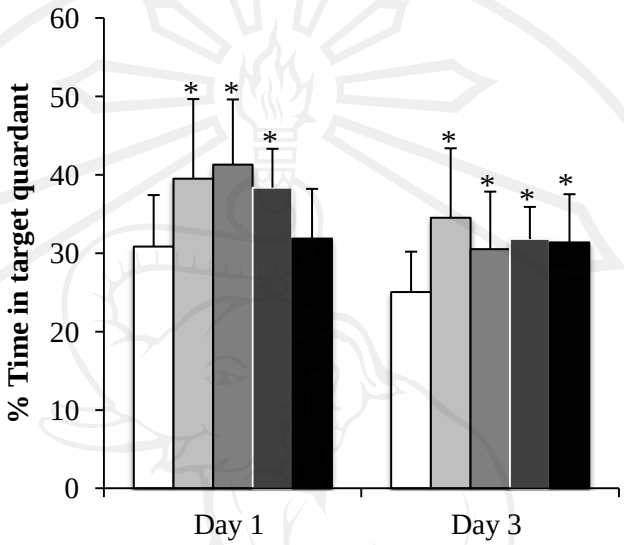

Figure 23 Time in target quadrant of the mice receiving i.p. scopolamine at the dose of 1.0 mg/kg (□), oral galantamine at the dose of 1 mg/kg (■), transdermal TD alkaloidal extract at the dose of 1,000 mg/kg (■), 500 mg/kg (■) and 250 mg/kg(■) in probe test ($n = 6$, $p < 0.05$).

<u>Part III</u> Preformulation study

The solubility of TD alkaloidal extract in various solvents was investigated. The results are shown in **Table 10**. TD alkaloidal extract was soluble in absolute ethanol and methanol; sparingly soluble in 95% ethanol, DMSO and acetone; slightly soluble in acetonitrile, isopropanol, butanol, PG, ethyl acetate, chloroform and dichloromethane; very slightly soluble in human serum and diethyl ether.

Table 10 Solubility of TD alkaloidal extract in various solvents.

Solvent	**Solvent amount (g) to dilute 1 g of TD alkaloidal extract**
absolute ethanol	13.30
methanol	15.20
95% ethanol	50.70
DMSO	61.40
acetone	89.60
acetonitrile	133.70
isopropanol	134.33
butanol	137.00
PG	145.04
ethyl acetate	162.00
chloroform	485.00
dichloromethane	876.00
human serum	2,200.00

Table 10 (Cont.)

Solvent	Solvent amount (g) to dilute 1 g of TD alkaloidal extract
diethyl ether	3,234.00
cetyl alcohol	>10,000
stearyl alcohol	>10,000
liquid parafin	>10,000
isopropyl myristate	>10,000
hexane	>10,000
Tween 20	>10,000
Tween 80	>10,000
Span 80	>10,000
PEG 200	>10,000
PEG 300	>10,000
PEG 400	>10,000
PEG 600	>10,000
glycerin	>10,000
PBS pH 7.4	>10,000
water	>10,000

The octanol-water partition coefficient is a physical property used extensively to describe a lipophilic or hydrophobic property of a compound. The partition coefficient was calculated as the ratio of TD alkaloidal extract concentrations in the octanol and aqueous phases at the equilibrium. Since measured values range from

$>10^{-14}$ to $<10^{+8}$ (at least 12 orders of magnitude), the logarithm (log *P*) is commonly used to characterize the value (92). The high value of log *P* represents to the hydrophobicity while the low value represents to the hydrophilicity. The importance of the partition coefficient of the penetrant as a factor in the measurement of *in vitro* percutaneous penetration has been reported since log *P* is correlated with permeation across the stratum corneum (93-94). Higher percutaneous penetration was found in the compounds with low log *P* (94). The calculated log *P* of TD alkaloidal extract was 3.03±0.07 (n = 2) which was in the proper range because it is generally accepted that the best drug candidates for passive adhesive transdermal patches must have adequate solubility in oil and water with log *P* value in the range of 1-3 (95). Currently most of the available transdermal drugs has the log *P* value in the range of 1-3 such as nicotine (log *P* = 1.17), scopolamine (log *P* = 2.09), nitroglycerin (log *P* = 2.15), clonidine (log *P* = 2.40) and rivastigmine (log *P* = 2.45) (96-98). However, log *P* values of some transdermal drugs excess 3 such as testosterone (log *P* = 3.32) estradiol (log *P* = 4.00) and fentanyl (log *P* = 4.05) (99-101). Therefore, TD alkaloidal extract which its log *P* was 3.03 would be a good candidate for transdermal application.

TGA and DSC were used for the study of thermal behavior of TD alkaloidal extract. TGA thermogram as shown in **Figure 24a** indicated the decompositions of the extract after exposure to high temperature. The decomposition of TD alkaloidal extract occurred in many step process as can be seen from the derivative of % weight lost. The isolated maximum weight losses were found at 48.72°C and 110.86°C. After that a cluster of maximum weight loss was found when the temperature was over 150°C. According to the first maximum weight loss at 48.72°C, weight of TD

alkaloidal extract decreased by 2.788% of the original. To understand the reason of weight lost, a more in-depth thermal behavior investigation was done by using DSC. DSC thermogram as shown in **Figure 24b** revealed a glass transition temperature (Tg) at 48.67°C. Therefore, the lost of TD alkaloidal extract might be related to the transition of the extract from a hard and brittle state to a molten or rubber-like state. According to the maximum weight loss at 110.86°C, the weight of TD alkaloidal extract was further decreased by 7.761%. A board endothermic peak found at 101.36°C in DCS thermogram, which was supposed to be the endothermic peak of water evaporated at around 100°C, was assumed to be one reason of the loss of weight. Finally, several exothermic peaks from DSC thermogram after 150.86°C were observed due to decompositions of the TD alkaloidal extract which were in a good agreement with the cluster of maximum weight loss that was found in TGA thermogram when the temperature was over 150°C. And the final weight of TD alkaloidal extract was about 72% of the original amount at 300°C.

The stability of TD alkaloidal extract in various conditions was investigated to see the effects of light, oxygen and temperature. The physical appearance of the TD alkaloidal extract which is brown solid did not change in all conditions throughout the stability study of 6 months. However, determination of TD alkaliodal extract by HPLC showed the differences as can be seen in **Figure 25**.

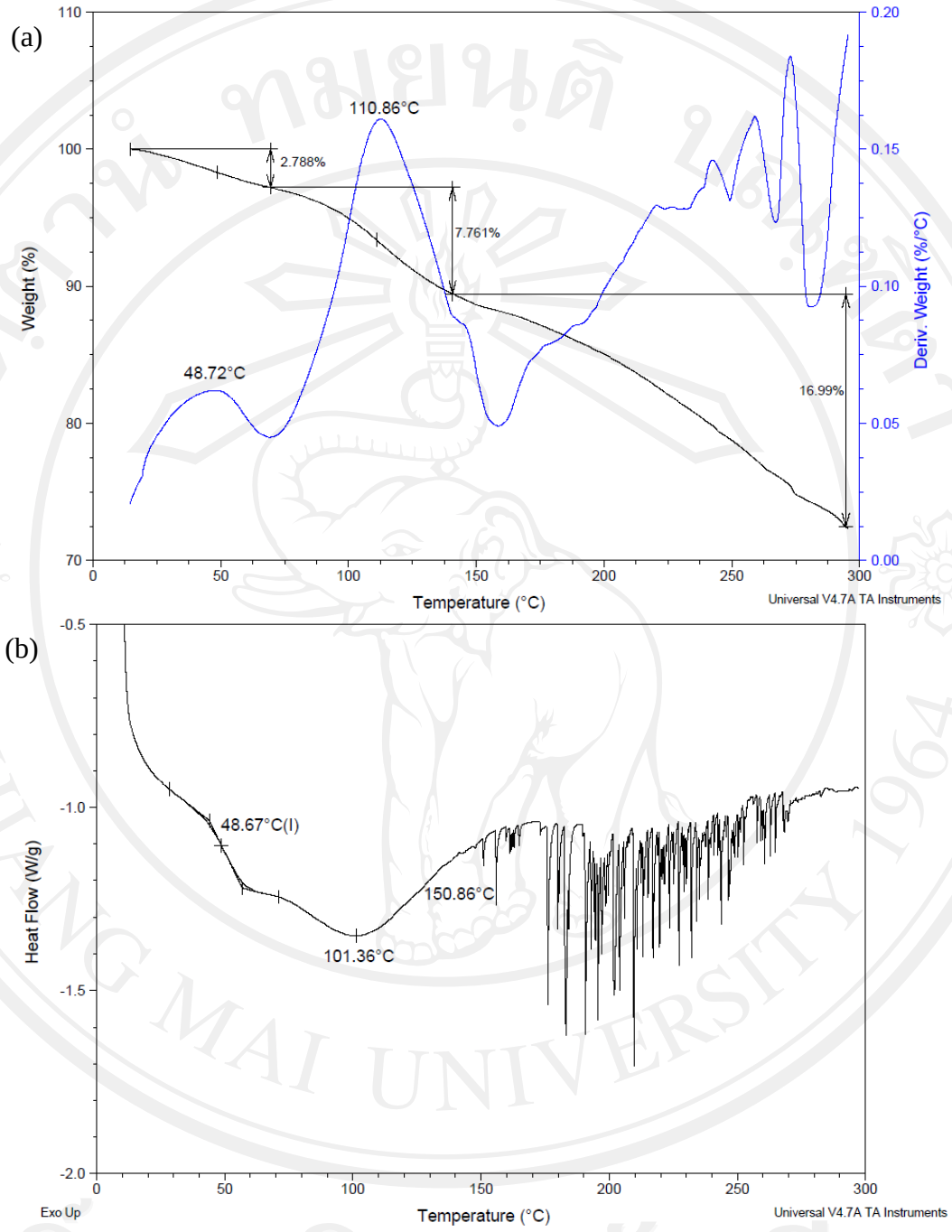

Figure 24 TGA thermogram (a) of TD alkaloidal extract displayed % weight lost (black) and derivative of % weight lost (blue) after heating the samples from 10°C to 300°C; DSC thermogram (b) of TD alkaloidal extract after heating the samples from 10°C to 300°C at a linear scanning rate of 10°C/min under a constant nitrogen purge.

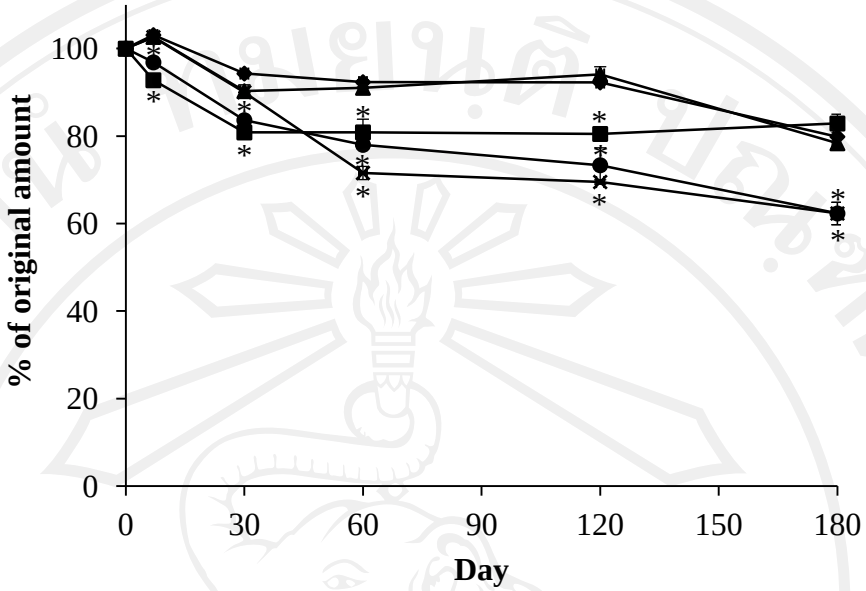

Figure 25 Graph of stability of TD alkaloidal extract stored in exposure to light (×), exposure to oxygen (■) or normal condition in the temperatures of 4°C (♦), 30°C (▲), and 45°C (●) for 180 days ($p < 0.05$).

The degradations were found when TD alkaloidal extract was stored without light and oxygen protection. The amount of TD alkaloidal extract when exposed to oxygen has exhausted since the first week of the storage and then gradually become lower. After one month of the storage, the amount almost constant around 80% of original. In the other hand, the amount of TD alkaloidal extract when exposed to light constant until one month of the storage, then it gradually decreased to 60% after six months. Therefore, the recommended storage condition of TD alkaloidal extract is light and oxygen protected. However, depletion of alkaloidal amount has been found in such conditions when the temperature was high (45°C). Consequently, storage in high temperature condition should also be avoided.

The anti-ChE of the TD alkaloidal extract has also been evaluated. **Figure 26** demonstrates the inhibitory activity against both AChE and BChE. The results indicated the constant in the activity in all storage conditions. The inconsistent with the above HPLC results might be resulted from the concentration of TD alkaloidal extract used in Ellman's assay. Since TD alkaloidal extract was a potent anti-ChE, the concentration used in the analyses maybe too high. Then it reached the maximum inhibition.

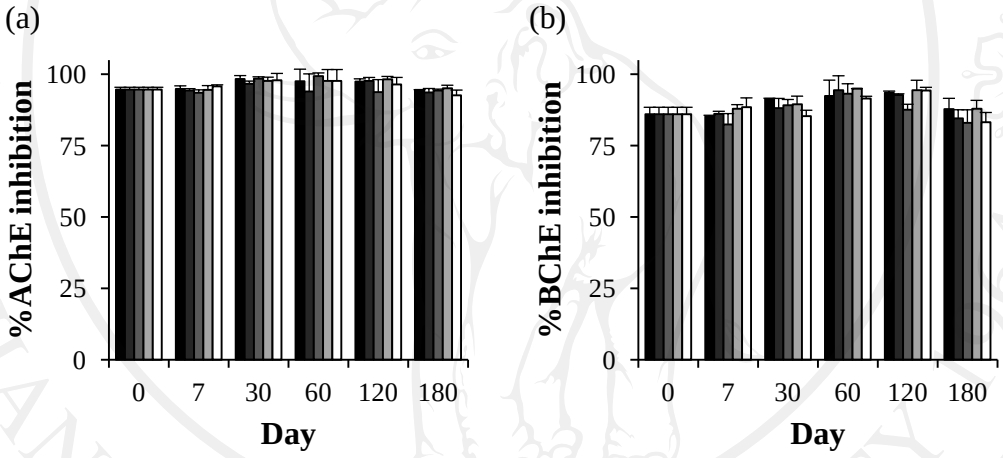

Figure 26 Inhibitory activities against AChE (a) and BChE (b) of 0.1 mg/mL TD alkaloidal extract when stored in light and oxygen protected condition at 30°C (■), exposure to light (■), exposure to oxygen (■) or protected condition in the temperatures of 4°C (■) and 45°C (□) for 180 days.

The cytotoxicity of TD alkaloidal extract was investigated by MTT assay which based on the reduction of a tetrazolium salt MTT by the living cell (102). The tetrazolium salt MTT is actively ingested by the cells and subsequent enzymatically converted from a yellow soluble form to a reddish purple formazan crystal. In case of

cell death, there was no reddish purple color produced since no enzyme to convert to those formazan crystals. Therefore, the reduction in reddish purple was used to indicate the death of cells. **Figure 27** shows dose-response curves of viability of PBMC and concentration of TD alkaloidal extract. The IC_{50} value was calculated from the plot. Blood samples were taken from three different donors for the triplicate study. TD alkaloidal extract possess the IC_{50} value of 7.54±4.76 mg/mL which is around 5.8×10^4 times when compare with the IC_{50} value against AChE (0.13 µg/mL).

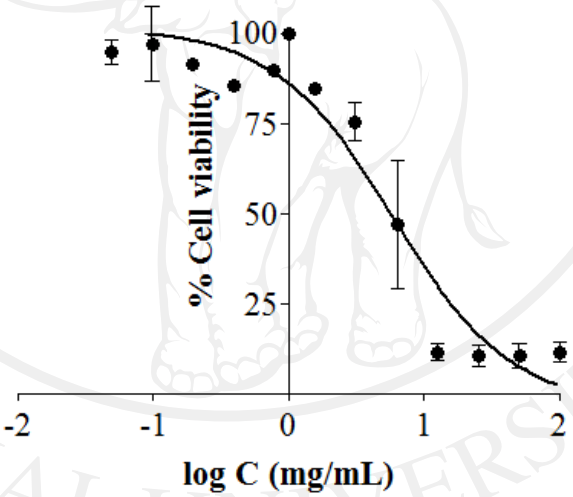

Figure 27 Dose-response curve of viability of PBMC versus concentration of TD alkaloidal extract.

<u>Part IV</u> Development of microemulsions containing TD alkaloidal extract

Transdermal drug delivery system represents the most successful non-oral systemic drug delivery since it promises many advantages over oral or intravenous administration (32). However, human skin provides an effective biological barrier to the permeation of most therapeutic agents. The principal barrier to transdermal drug delivery is the stratum corneum, the outer most layer of the skin comprising keratin-rich cells embedded in multiple lipid bilayers which is lipophilic character and intrinsic tortuosity (34, 37). Human skin is designed to keep 'our insides in and the outsides out' to prevent the body from losing water into the environment and to block the entry of exogenous agents (103-104). Several methods including physical and chemical have successfully resulted in elevated levels of drugs delivered across the skin (104). However, much interest has been focused on methods of increasing stratum corneum permeability by the use of penetration enhancers (also called sorption promoters or accelerants), the substances that facilitate the absorption of penetrant through the skin by temporarily diminishing the impermeability of the skin (103, 105). Several kinds of compounds have been evaluated as penetration enhancers include water, sulphoxides, azone, pyrrolidones, fatty acids, alcohols, fatty alcohols, glycols, surfactants, urea, essential oils, terpenes, terpenoids, phospholipids, solvents at high concentrations and metabolic interventions (103). Therefore, essential oil which is a rich source of terpenes and terpenoids was selected to be an oil phase in microemulsion.

Firstly, several essential oils from Thai plants have been isolated and evaluated for the yield amount as well as AChE and BChE inhibitions. The names of all plants are list in **Table 11** while the yields are shown in **Figure 28**.

Table 11 Species, family and plant part analyzed of essential oils.

Species	Family	Plant part analyzed
Centella asiatica	Apiaceae	Whole plant
Polyscias fruticosa	Araliaceae	Leaf
Eupatorium odoratum	Asteraceae	Whole plant
Cymbopogon citratus	Gramineae	Stem
Ocimum sanctum	Lamiaceae	Leaf
Ocimum canum	Lamiaceae	Whole plant
Ocimum gratissimum	Lamiaceae	Leaf
Melissa officinalis	Lamiaceae	Leaf
Ocimum basilicum	Lamiaceae	Leaf
Cinnamomum bejolghota	Lauraceae	Leaf
Piper sarmentosum	Piperaceae	Leaf
Polygonum odoratum Lour .	Polygonaceae	Whole plant
Citrus hystrix	Rutaceae	Leaf
		Fruit peel
Citrus aurantifolia	Rutaceae	Leaf
		Fruit peel
Citrus maxima	Rutaceae	Leaf
		Fruit peel
Citrus reticulata Blanco cv. Shogun	Rutaceae	Leaf
		Fruit peel
Citrus reticulata var. Fremont	Rutaceae	Leaf
		Fruit peel

Table 11 (Cont.)

Species	Family	Plant part analyzed
Alpinia galanga	Zingiberaceae	Rhizome
Zingiber officinale	Zingiberaceae	Rhizome
Zingiber cassumunar	Zingiberaceae	Rhizome

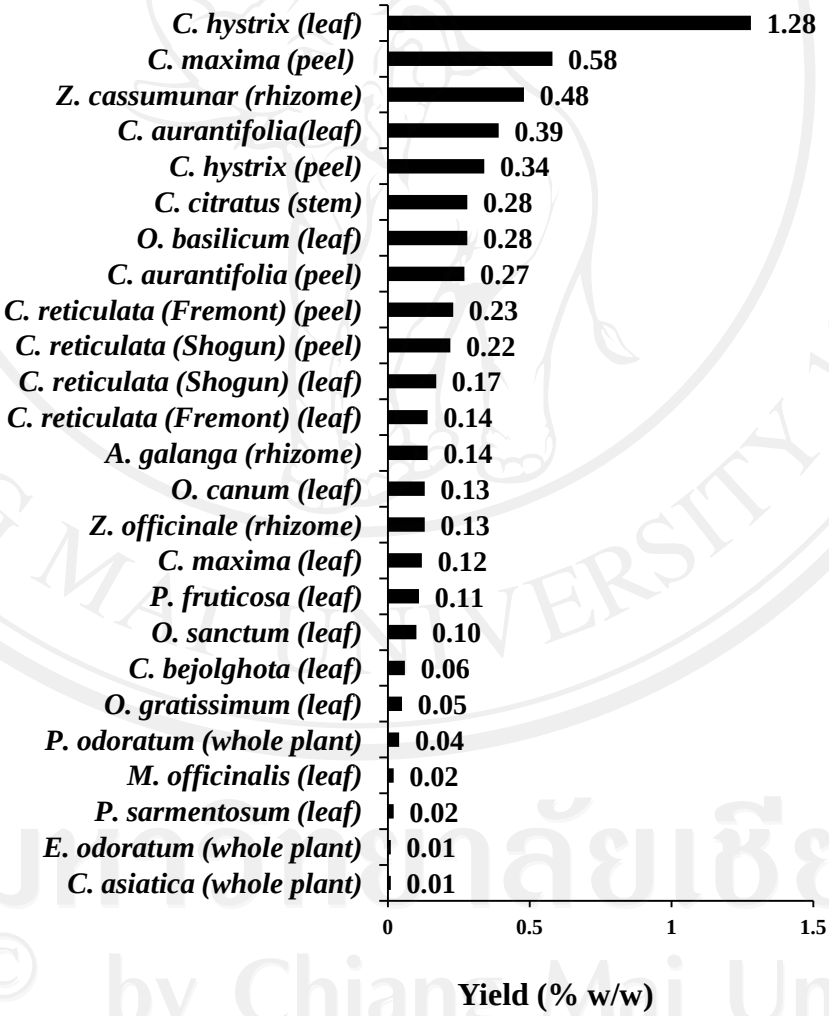

Figure 28 The yield of each essential oil (% w/w).

Although one of the desirable properties for penetration enhancers is no pharmacological activity within the body, the inhibitory activities against AChE and BChE of these essential oils were evaluated. The synergistic effect or at least additional effect would be a satisfied result. As can be seen in **Figure 29**, essential oil from leaf of *M. officinalis* exhibits high AChE and BChE inhibition. However, the yield of this oil was very low (0.02% w/w). Therefore, the further usage of this oil would encounter with problems such as large amount of raw plant needed, long time to distillate the essential oil and also the high cost of production. Finally, the essential oils were selected by the availability as well as the cost and the important consideration would be % yield. The essential oil from *C. citratus* and *Z. cassumunar* were selected for the further study according to the above reasons.

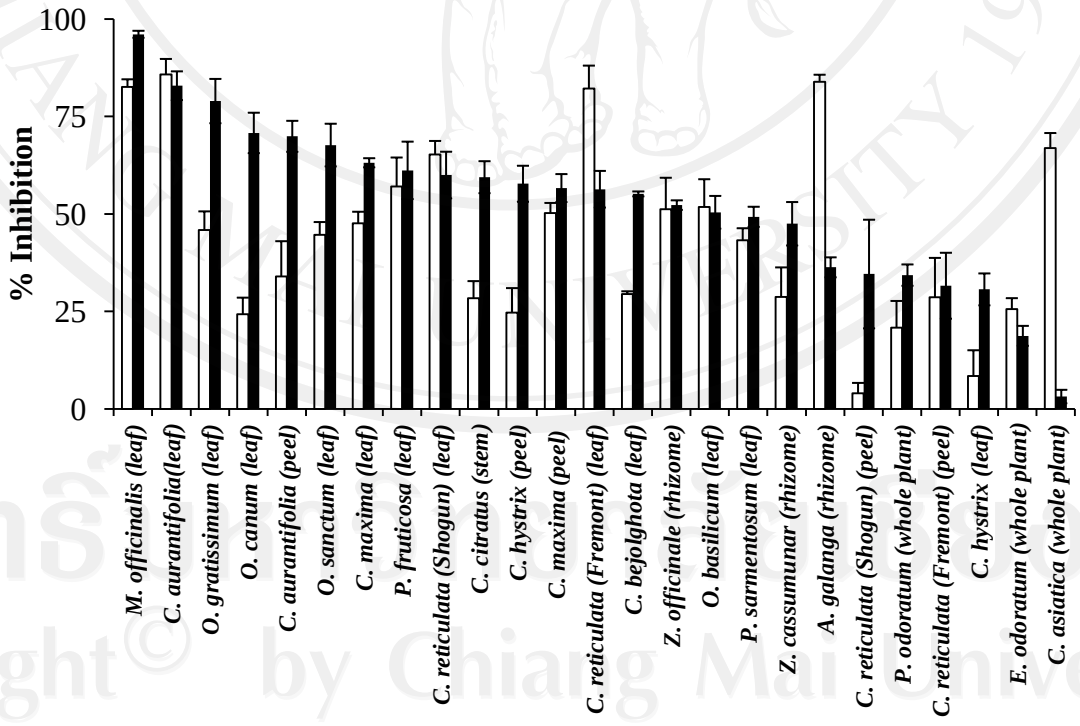

Figure 29 Inhibitory activities of 0.1 mg/mL essential oils against AChE (□) and BChE (■).

According to microemulsion development, pseudoternary phase diagrams were constructed using a water titration method in order to investigate the microemulsion regions of different systems. Before incorporating the TD alkaloidal extract, blank microemulsions were prepared and characterized. Various factors including oil type, surfactant type, co-surfactant type, surfactant to co-surfactant ratio, pH and ionic strength of the aqueous phase were investigated. In this part of the study, the results would be divided into (I) microemulsion of *C. citratus* oil and (II) microemulsion of *Z. cassumunar* oil.

(I) Microemulsion of *C. citratus* oil

Four nonionic surfactants (Brij 97, Triton X-114, Tween 20 and Tween 85; structures shown in **Figure 30**) were selected for the preparation of microemulsions of *C. citratus* oil because of their low toxicity (43, 106).

(a)

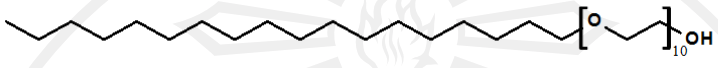

(b)

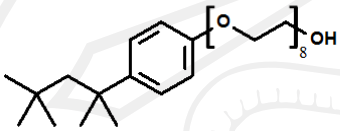

(c)

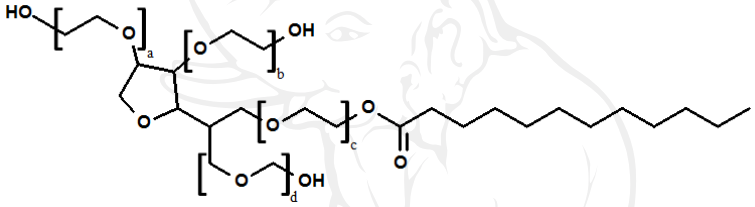

(d)

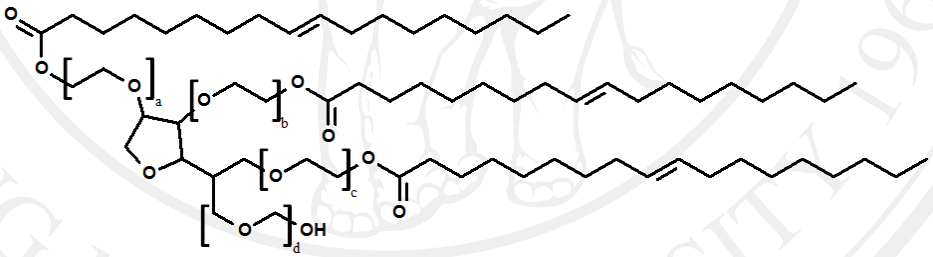

Figure 30 Chemical structures of the used surfactants: Brij 97 (a), Triton X-114 (b), Tween 20 (c) and Tween 85 (d).

Surfactant and co-surfactant (Smix) are apart from oil and water necessary constituents in microemulsions. Increasing amounts of Smix allow the microemulsions to contain greater amount of active oil as shown in **Figure 31**. However, the types of surfactants also play a dominant role. To prepare microemulsions with the same amount of active oil, different amounts of Smix were

needed. For example, 10% of *C. citratus* oil needs about 30%, 45%, 40% and 70% of Smix for Brij 97, Triton X-114, Tween 20 and Tween 85, respectively. Moreover, the area existing in the phase diagram of these four surfactants is obviously distinct from each other. Despite the fact that two surfactants having the same HLB (Brij 97 and Triton X-114, **Figure 30a** and **30b**) shows differences in pseudoternary phase diagrams, the lower the critical micelle concentration (CMC) of a surfactant, the less is needed to form a microemulsion (107). Thus at the same concentration, Triton X-114 should be a better surfactant to create microemulsions. Surprisingly, our results show that Brij 97 is a better surfactant to form microemulsions than Triton X-114 although its CMC value is greater, indicating that the molecular geometry of the surfactants, which is very different for these two surfactants, may play a role in microemulsion formation (108). However, it is known that more bulky surfactant molecules are able to form films that are more stable against rupture (109). This observation can clarify the better ability in microemulsion formation of Brij 97, which has higher molecular weight and is more bulky than Triton X-114. **Figure 31** also shows that the microemulsion forming ability of Tween 85 was much less pronounced than those of the structurally related Tween 20, which may be explained by the higher HLB value of the latter surfactant. Since the HLB of a surfactant has been suggested a parameter to explain the stabilization properties of some microemulsion systems (110). However, while it is known that the higher the HLB value of a surfactant, the easier it forms O/W emulsions (111-112), there is no direct correlation between the HLB value of the surfactants and their ability of forming microemulsions. For example, Brij 97 has an HLB value of 12.4 and has the largest microemulsion area in the phase diagrams of this study, whereas the HLB value of Tween 85 is only slightly

lower (11.4) but the use of this surfactant resulted in a substantially smaller microemulsion area. Given its good ability to prepare microemulsions with *C. citratus* oil, its low toxicity (113) and its cost effectiveness, Tween 20 was selected for further microemulsion studies.

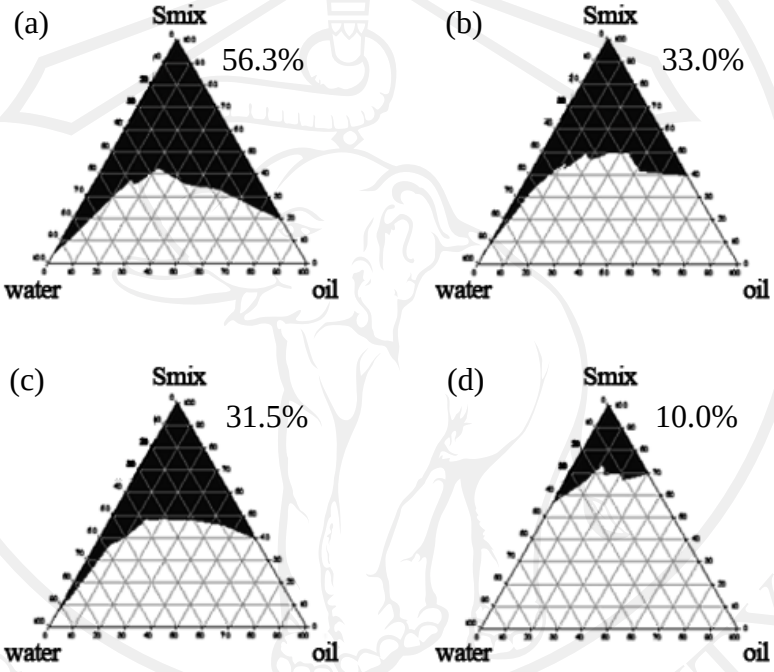

Figure 31 Pseudoternary phase diagrams of *C. citratus* oil/water/surfactant/co-surfactant mixtures containing Brij 97 (a), Triton X-114 (b), Tween 20 (c) and Tween 85 (d). The dark area represents the region of microemulsion.

The use of a single surfactant is unlikely to reduce the interfacial tension between oil and water to form stable microemulsions, and therefore the addition of a co-surfactant is generally required (114). It has previously been shown that the type of co-surfactant and the ratio of surfactant/co-surfactant affect the formation of

microemulsions (115). Ethanol and hexanol were used as co-surfactants in this study (**Figure 32**).

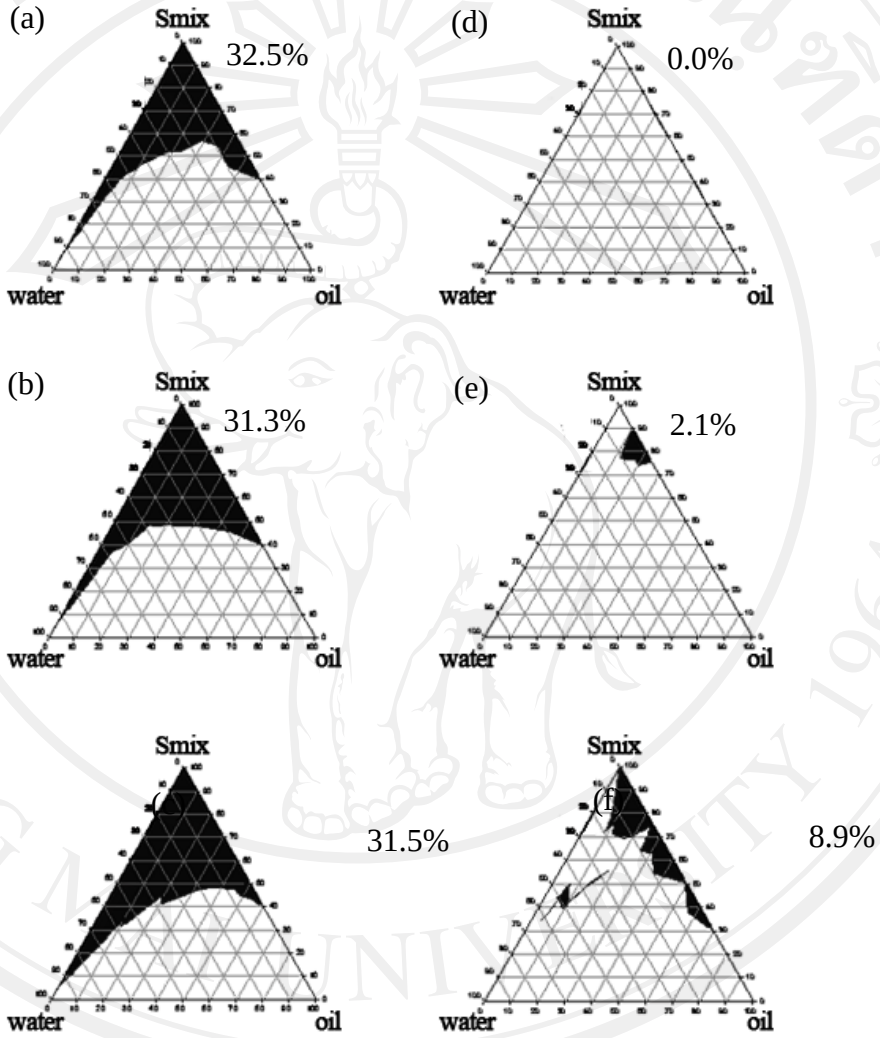

Figure 32 Pseudoternary phase diagrams of *C. citratus* oil using surfactant system of Tween 20: ethanol with a weight ratio of 1:2 (a), 1:1 (b), and 2:1 (c) and Tween 20: hexanol of 1:2 (d), 1:1 (e), and 2:1 (f). The dark area represents the region of microemulsion.

Figure 32 shows that the microemulsion regions of the systems with ethanol are much larger than those with hexanol. Ethanol is more hydrophilic than hexanol and it is therefore likely that hexanol will be essentially present in the oil phase while ethanol partitions over the aqueous and oil phase. Therefore, the interfacial tension between the oil and aqueous phase in the system with ethanol is lower than that in the corresponding systems with hexanol. This in turn favours the formation of small emulsified droplets. Further, it has been reported that ethanol is able to insert into the interfacial layer and forms a tight interfacial film (116). This also might contribute to the better performance of ethanol compared to hexanol to create microemulsions.

It has been shown that the region of existence of microemulsions as well as the size of the emulsified droplets may be affected by electrolytes (117). To investigate whether the ionic strength of the aqueous phase affected microemulsions of *C. citratus* oil, NaCl and $CaCl_2$ were employed as monovalent and divalent electrolytes, respectively. The results of **Figure 33** show that the phase diagrams of mixtures containing 0.5 M of either NaCl or $CaCl_2$ are not different than that from the mixtures containing no salt. However, at high salt concentration (1.0 M NaCl or $CaCl_2$) the region of existence of microemulsion became smaller. Likely, the PEG chains of Tween 20 are dehydrated in the high salt solution which adversely affects its surfactant activity, therefore requiring higher concentrations of surfactant to yield stable microemulsions.

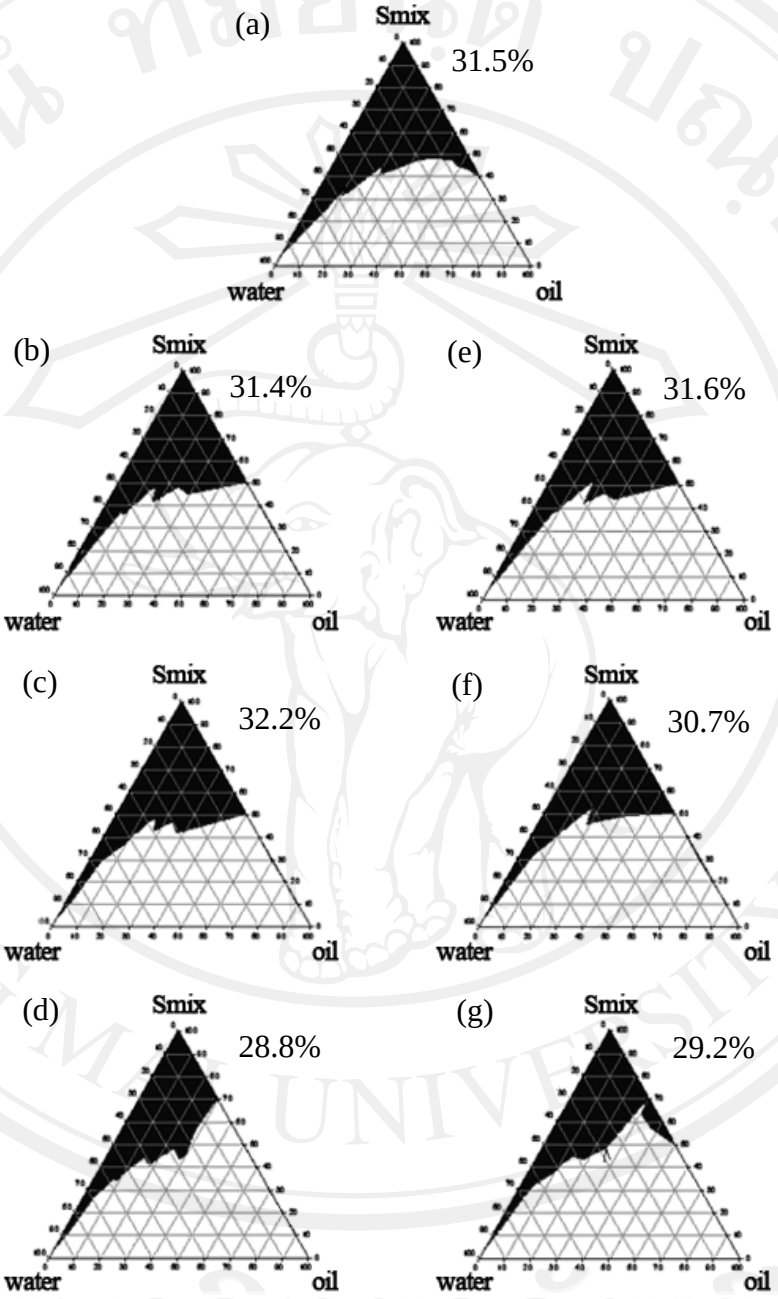

Figure 33 Pseudoternary phase diagrams of *C. citratus* oil using 2:1 mixture of Tween 20:ethanol as surfactant system with an aqueous phase of water (a), 0.1 M NaCl (b), 0.5 M NaCl (c), 1.0 M NaCl (d), 0.1 M $CaCl_2$ (e), 0.5 M $CaCl_2$ (f) and 1.0 M $CaCl_2$ (g). The dark area represents the microemulsion region.

The pH of the buffer had no significant effect on the phase diagrams (results are shown in **Figure 34**). This is in line with expectations and previous papers (112, 118), since non-ionic surfactants were used to stabilize the emulsions.

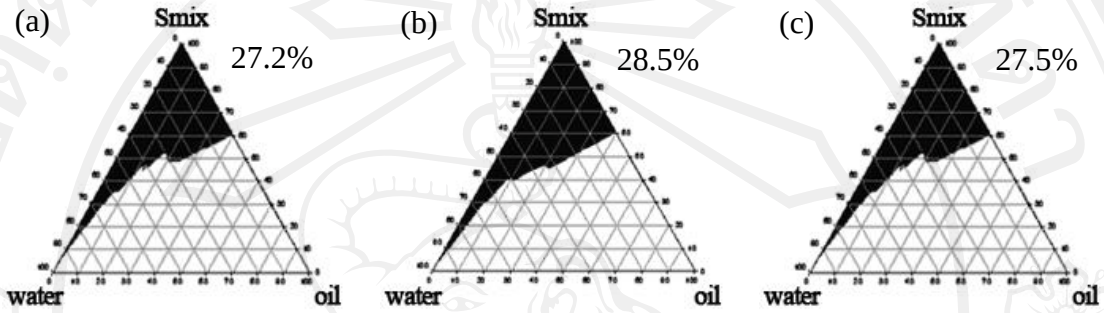

Figure 34 Pseudoternary phase diagrams of *C. citratus* oil using 2:1 mixture of Tween 20:ethanol as surfactant system with an aqueous phase of water pH 4.0 (a), 6.0 (b), and 8.0 (c). The dark area represents the microemulsion region.

Finally, the selected microemulsions were then characterized for the particle size and electrical conductivity. The microemulsion formulations selected for the size and zeta potential analysis were composed of 10% of *C. citratus* oil, 40% of water and 50% of Smix (surfactant:ethanol = 2:1), using Brij 97, Triton X-114 and Tween 20 as surfactant. But in the system of Tween 85, 80% of Smix was used because 50% was not enough to form microemulsions. PCS analysis showed that the particles stabilized by Brij 97, Tween 20, Triton X-114 and Tween 85 were 9.5±0.1, 91.9±4.4, 11.4±0.1 and 78.6±3.0 nm, respectively. This means that indeed microemulsions were formed because their sizes range from 5 to 100 nm (118, 47). The particle size distributions were intermediate (PDI < 0.3). Of the investigated surfactants, Brij 97 and Triton X-114 gave the smallest emulsified droplets. There is however no relation

between the particle size of the emulsified droplets and the physicochemical characteristics of the used surfactants.

Electrical conductivity is frequently used to investigate structural changes in oil/water/surfactant systems (119-120). As the data of **Figure 33** shows that low concentration of salt had no effect on microemulsions composed of water/*C.citratus* oil/Tween 20/ethanol mixture, 0.1 M NaCl solution was hence used as an aqueous phase. The relationship between aqueous phase ratio and conductivity values is shown in **Figure 35**. As long as aqueous phase ratio was <0.2, the conductivity value was very low. This is in line with expectations since at low water volume fractions, the oil forms the continuous phase. However, the conductivity values substantially increased at an aqueous phase ratio above 0.2 and substantially increased when the aqueous phase volume fraction was > 0.5 which points to a transition from a W/O emulsion to an O/W microemulsion (42, 108).

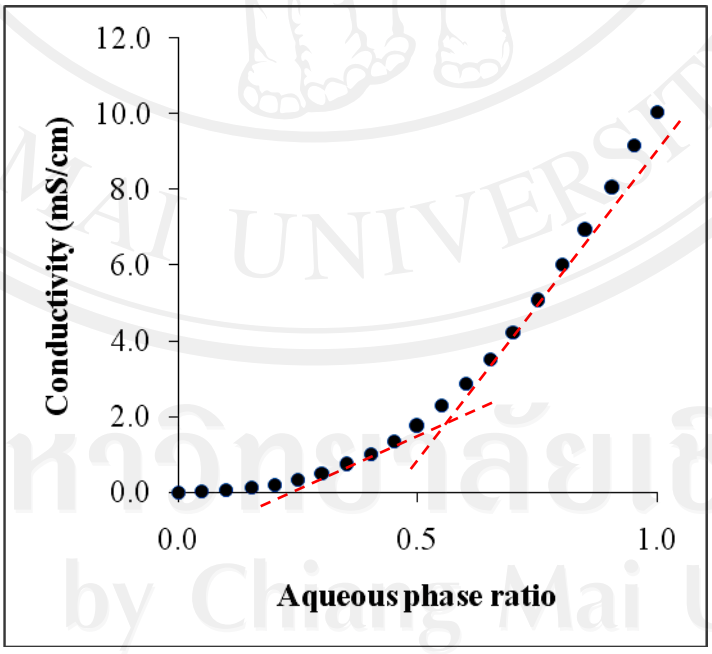

Figure 35 Conductivity versus aqueous phase ratio of formulations containing *C. citratus* oil/Smix = 1:9 in which Smix is a mixture of Tween 20 and ethanol (2:1).

(II) Microemulsion of *Z. cassumunar* oil

Nonionic surfactants were employed in this study since they show low irritancy and low toxicity (113) while ethanol was used as a co-surfactant because of its amphiphilic nature and low MW which can influence the formation of microemulsions by both interfacial and bulk effects (121). The phase behavior of *Z. cassumunar* oil/surfactant/co-surfactant/water system was represented in a pseudoternary phase diagram, in which *Z. cassumunar* oil is one component, another one is water, and the third component is Smix, which is a mixture of surfactant and co-surfactant. The ternary phase diagram was constructed adopting a simple titration method. Smix, in which the surfactant and co-surfactant mass ratio was fixed, was first prepared by combining the required mass of the surfactant and co-surfactant. Then an appropriate quantity of *Z. cassumunar* oil was introduced into the emulsifier and water was the titration component. The phase boundary was noted by observing the transition from turbidity to transparency or from transparency to turbidity. **Figure 36** shows microemulsion region of three phase diagram composing of different nonionic surfactants when ethanol was used as a co-surfactant in a ratio of 2:1. Tween 20 and Triton X-114 showed a very close microemulsion region with the different patterns. However, Triton X-114 showed the largest microemulsion region among three different surfactants. The results could be explained by the CMC that is the concentration at which micelles first appear in the solution. CMC can indicate the number of surfactant to form the micelle. Below this critical value, additional surfactant added to solution remains in monomeric form, and above this, essentially all additional surfactant forms micelles (122). The CMC of Tween 20 and Triton X-114 are 0.500 and 0.168 mg/mL, respectively (123). Therefore, Triton X-114 was

needed in the smaller amount to form the micelle. However, Tween 20 tended to be more suitable surfactant than Triton X-114 at higher volume of the aqueous phase. Microemulsion region can be found in the phase diagram of Tween 20 when almost 100% of water was in the system. Microemulsion formation of Triton X-114 was not found when the water volume exceeded 80%. This could be the responsibility of the HLB values of each surfactant. Tween 20 exhibited higher HLB value than that of Triton X-114 (16.7 and 12.4, respectively), therefore, O/W microemulsion were formed easier (122, 111).

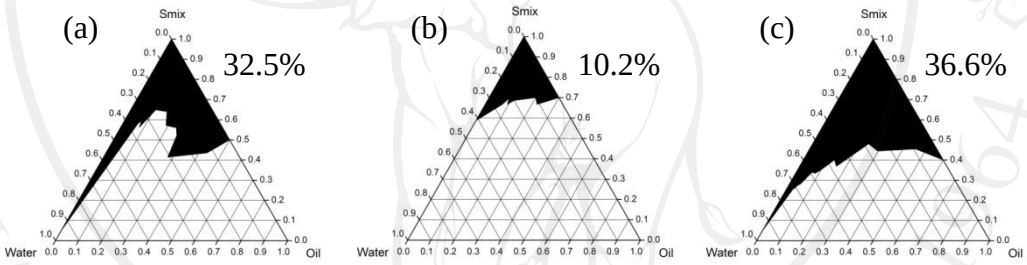

Figure 36 Pseudoternary phase diagrams of *Z. cassumunar* oil/water/surfactant/co-surfactant mixtures containing Tween 20 (a), Tween 85 (b) and Triton X-114 (c). The dark area represents the region of microemulsion.

Co-surfactants can reduce the surface tension and increase the flexibility of the interface by partition themselves among the oil, water, and interface domains (124) which lead to the spontaneously formed microemulsion (125). Since co-surfactant participates in a micelle and adjusting the polarity of water and oil, it thus affects the system of phase behavior and nature of the microemulsion components (126). Therefore, the study of suitable co-surfactant would be fascinated. The effect of chain

length of linear alcohols on the phase behavior of microemulsion systems were investigated by using ethanol, n-propanol and cetyl alcohol. **Table 12 and 13** show phase diagrams as well as percentage of microemulsion region occurred from various type of co-surfactant mixed with Triton X-114 or Tween 20.

The results indicate that cetyl alcohol, the longest alkyl chain alcohol in this study, gave very sparse microemulsion region with Triton X-114 while gave no region with Tween 20. Moreover, the microemulsion regions in the phase diagrams of ethanol were larger than that of n-propanol. These results were in accordance with the previous study of Alany *et al*. (2000) which indicated that microemulsion region in the phase diagram reduced upon increasing the chain length of alkane alcohol (121). The branch chain of alcohol also affected the formation of microemulsion since n-propanol gave a trend of greater microemulsion regions in the phase diagram of Tween 20 than that of isopropanol. A likely explanation is that the complicated co-surfactant cannot form microemulsion properly if the structure of surfactant is so complex (126). However, the branched co-surfactant was superior to the linear co-surfactant in the system of Triton X-114. Therefore, we should consider the structure of both surfactant and co-surfactant and select the match couple for the microemulsion formation.

The effect of hydroxyl group numbers on the phase behavior was also investigated. Isopropanol was selected as a representative of alkane mono-ol when PG and glycerin represented to alkane diol and triol, respectively. The results are also shown in **Table 12** and **13**. In the system of Triton X-114, glycerin was not a good co-surfactant and the microemulsion region nearly disappeared with glycerin because of its high hydrophilic property. In the other hand, PG and isopropanol were

appropriated to form microemulsion with Triton X-114 since they gave larger area in the phase diagram. The results were also the same as the system of Tween 20. Moreover, PG showed higher performance in microemulsion formation when compared with PEG 400 because of its compact molecule (121). Therefore, PG was selected as a co-surfactant for the further investigations because it gave a large area of microemulsion region in the phase diagram as well as its non-volatile property.

Electrolyte was believed to have an effect on the region of microemulsions in the phase diagram because it affected on the size of the emulsified droplets (117). **Figure 37** and **38** exhibits the effects of electrolytes on microemulsion system of Triton X-114 and Tween 20, respectively. In the present study, NaCl was employed as a monovalent salt while $MgCl_2$ was employed as a divalent salt in the investigation of the effects on existent microemulsion regions. The results indicated that both electrolytes affected the regions. Moreover, the higher concentration of salts, the lower microemulsion regions were found. Because the salting effect of divalent electrolyte (Mg^{2+}) was higher than that of monovalent electrolyte (Na^{+}) (127).

In addition, the pH effects were also investigated and the results are shown in **Figure 39**. The pH exhibited no effect on the microemulsion region of *Z. cassumunar* oil system. Therefore, we can conclude that microemulsion system comprising of *Z. cassumunar* oil/Tween 20/PG/water and the system of *Z. cassumunar* oil/Triton X-114/PG/water were hardly affected by variation of the pH but could be affected by the high ionic strength of the aqueous phase.

Table 12 Microemulsion region (%) of *Z. cassumunar* oil using surfactant system of Triton X-114 with various weight ratio of surfactant to co-surfactant. The dark area represents the region of microemulsion.

Co-surfactant	Triton X-114: co-surfactant ratio		
	2 : 1	**1 : 1**	**1 : 2**
Mono-ol alcohol			
Ethanol	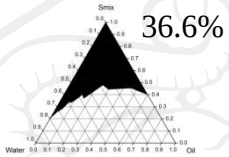 36.6%	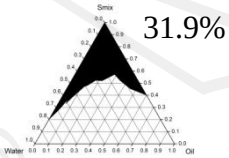 31.9%	 29.8%
Propan-1-ol	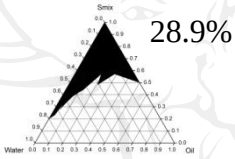 28.9%	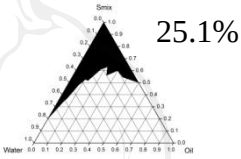 25.1%	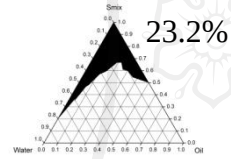 23.2%
Propan-2-ol	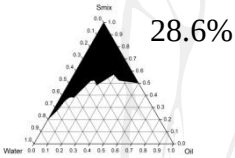 28.6%	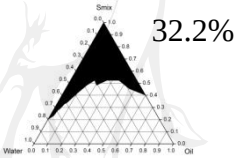 32.2%	 30.2%
Cetyl alcohol	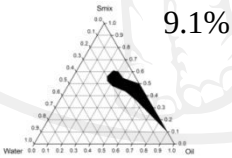 9.1%	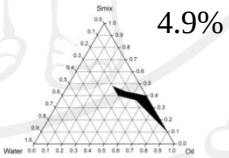 4.9%	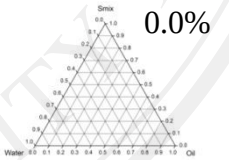 0.0%
Diol alcohol			
PG	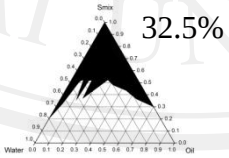 32.5%	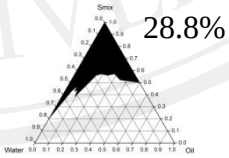 28.8%	 26.0%
PEG400	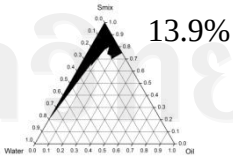 13.9%	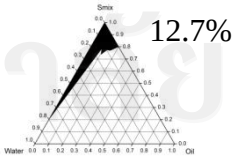 12.7%	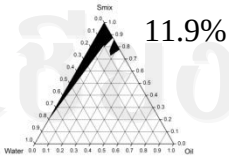 11.9%
Triol alcohol			
Glycerin	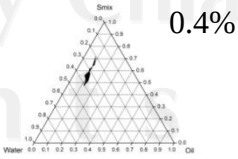 0.4%	 0.1%	 0.0%

Table 13 Microemulsion region (%) of *Z. cassumunar* oil using surfactant system of Tween 20 with various weight ratio of surfactant to co-surfactant. The dark area represents the region of microemulsion.

Co-surfactant	Tween 20 : co-surfactant ratio		
	2 : 1	**1 : 1**	**1 : 2**
Mono-ol alcohol			
Ethanol	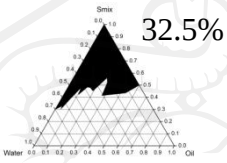 32.5%	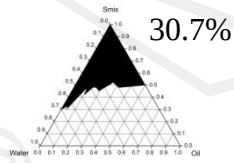 30.7%	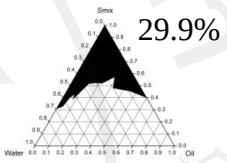 29.9%
Propan-1-ol	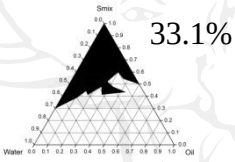 33.1%	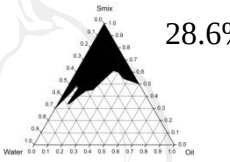 28.6%	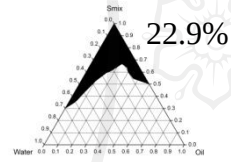 22.9%
Propan-2-ol	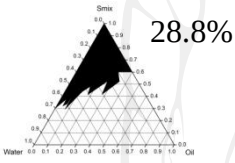 28.8%	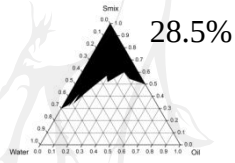 28.5%	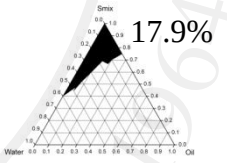 17.9%
Cetyl alcohol	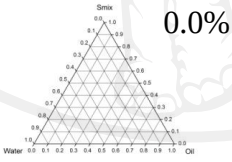 0.0%	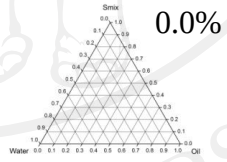 0.0%	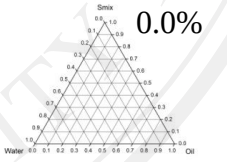 0.0%
Diol alcohol			
PG	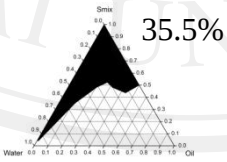 35.5%	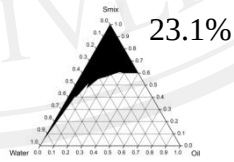 23.1%	 13.2%
PEG400	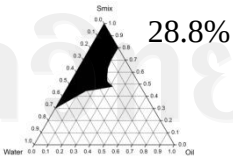 28.8%	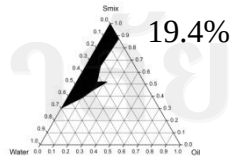 19.4%	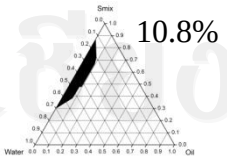 10.8%
Triol alcohol			
Glycerin	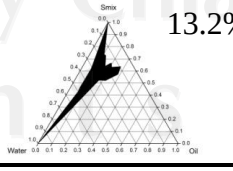 13.2%	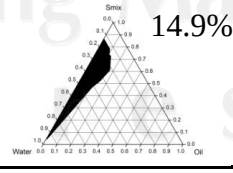 14.9%	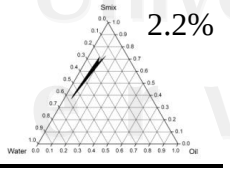 2.2%

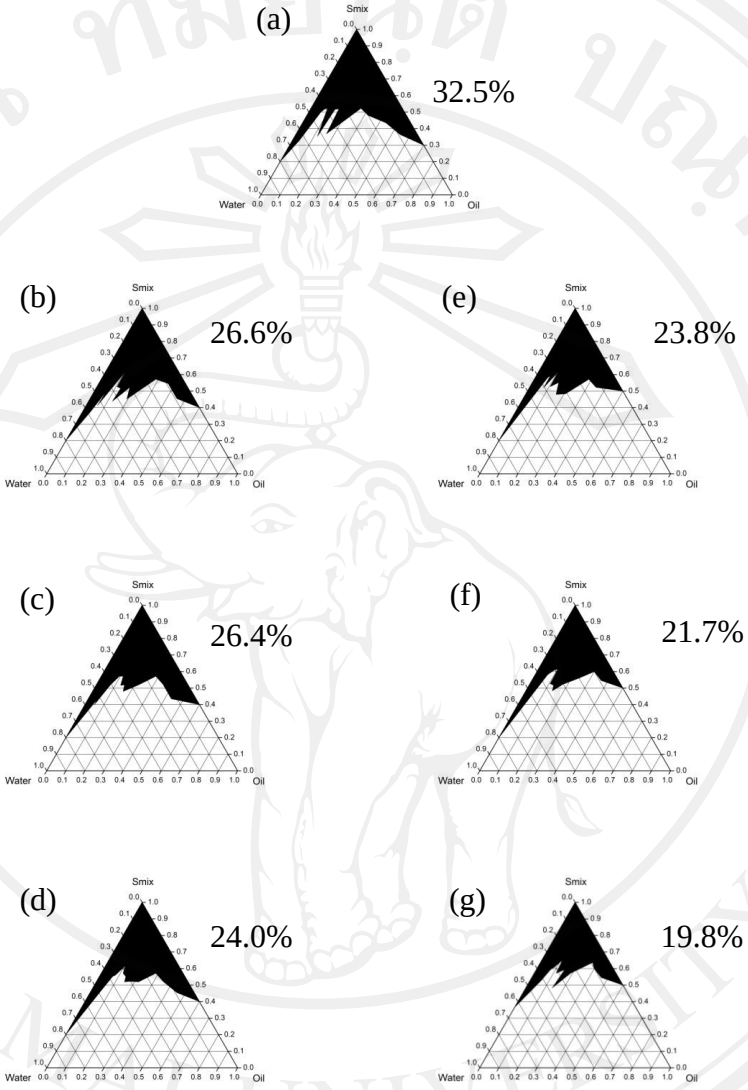

Figure 37 Pseudoternary phase diagrams of *Z. cassumunar* oil using 2:1 mixture of Triton X-114 : PG as surfactant system with an aqueous phase of water (a), 0.1 M NaCl (b), 0.5 M NaCl (c), 1.0 M NaCl (d), 0.1 M $MgCl_2$ (e), 0.5 M $MgCl_2$ (f) and 1.0 M $MgCl_2$ (g). The dark area represents the microemulsion region.

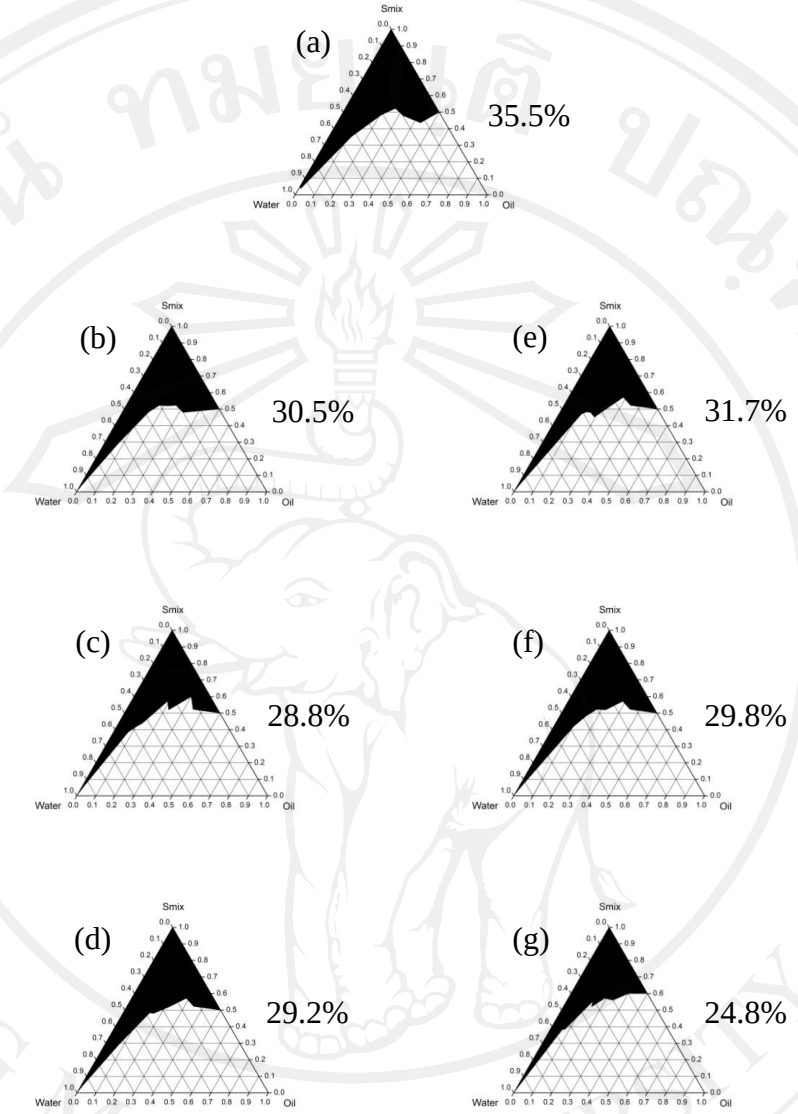

Figure 38 Pseudoternary phase diagrams of *Z. cassumunar* oil using 2:1 mixture of Tween 20 : PG as surfactant system with an aqueous phase of water (a), 0.1 M NaCl (b), 0.5 M NaCl (c), 1.0 M NaCl (d), 0.1 M $MgCl_2$ (e), 0.5 M $MgCl_2$ (f) and 1.0 M $MgCl_2$ (g). The dark area represents the microemulsion region.

In addition, the pH effects were also investigated and the results are shown in **Figure 39**. The pH exhibited no effect on the microemulsion region of *Z. cassumunar* oil system. Therefore, we can conclude that microemulsion system comprising of *Z.*

cassumunar oil/Tween 20/PG/water and the system of *Z. cassumunar* oil/Triton X-114/PG/water were hardly affected by variation of the pH but could be affected by the high ionic strength of the aqueous phase.

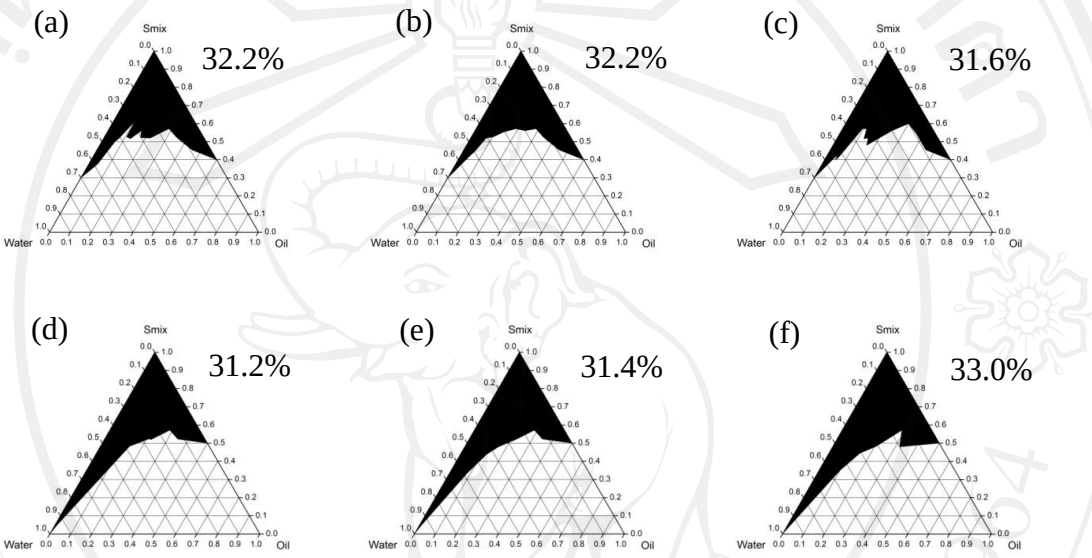

Figure 39 Pseudoternary phase diagrams of *Z. cassumunar* oil using 2:1 mixture of Triton X-114 : PG as surfactant system with an aqueous phase of water pH 4.0 (a), 6.0 (b) and 8.0 (c) and pseudoternary phase diagrams of *Z. cassumunar* oil using 2:1 mixture of Tween 20 : PG as surfactant system with an aqueous phase of water pH 4.0 (d), 6.0 (e) and 8.0 (f). The dark area represents the region of microemulsion.

Finally, twenty formulations along dilution line I and II from the pseudoternary phase diagram of *Z. cassumunar* oil/Triton X-114/PG/water as shown in **Figure 40** were selected for the further characterizations. Line I and II represented to the systems with oil/Smix ratio of 1:9 and 2:8, respectively.

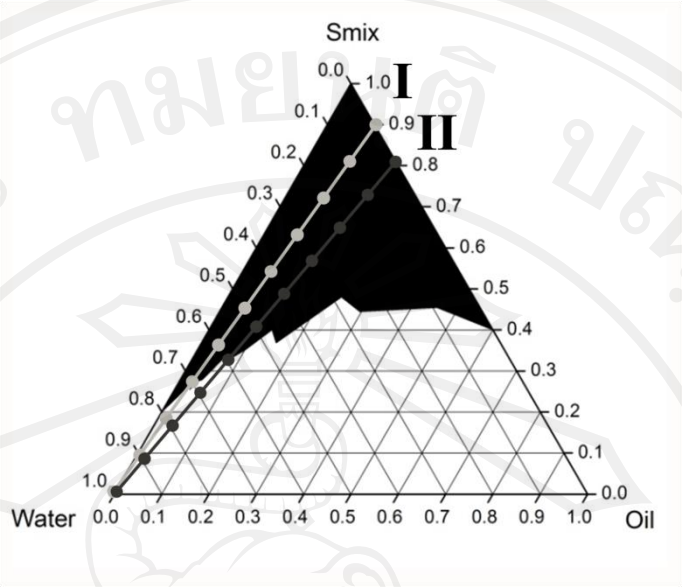

Figure 40 Pseudoternary phase diagram of *Z. cassumunar* oil/Triton X-114/PG/water using 2:1 mixture of Triton X-114: PG as surfactant system. Line I represented the mixture of oil and Smix in a ratio of 1:9, whereas the line II represented the mixture of oil and Smix in a ratio of 2:8. Each spot on the line represented to the formulations with 10% of water increased.

The particle size of the one-phase systems containing *Z. cassumunar* oil /Smix of 1:9 and 2:8 was found to be 15 to 55 nm as shown in **Table 14**. The particle sizes were so small and well within the microemulsion range (128-130). The small size of internal phase droplets was explained by the fact that the surfactant causes the interfacial film to stabilized and condense while the addition of co-surfactant causes the film to be expanded (131). The result also demonstrated that the nanosized internal phase droplets of the system with *Z. cassumunar* oil/Smix ratio of 1:9 could be obtained only when the water amount was less than 80%. Adding water up to 80% or more gave the system of two-phase coarse emulsion. For the system comprising 2:8 ratio of *Z. cassumunar* oil/Smix, the nanosized droplets were formed when the water

was not more than 50%. Moreover, the system consisted of 60-80 % water appeared as gel-like structure where phase separation occurred when more than 80% of water was added.

Table 14 Internal droplet size of microemulsion (nm).

% Water	ZC oil : mix ratio	
	1:9	2:8
10	55.74±3.53	55.57±4.83
20	23.88±1.44	43.12±7.42
30	27.86±2.42	22.32±0.33
40	15.47±0.02	32.60±2.38
50	17.43±0.11	35.35±3.38
60	21.56±0.04	ND
70	44.07±0.37	ND
80	ND	ND
90	ND	ND

ND: not defined because of over the detection range of PCS

The microstructure analysis was done by PLM which is the best way to distinguish lamellar liquid crystals from microemulsions and should always be a standard tool in the investigation of microemulsions (132). The differentiation of microemulsions from a liquid crystal was undertaken. Microemulsion is the isotropic system with non birefringence, therefore, no textures can be seen under the PLM. Microemulsions were defined in the system with *Z. cassumunar* oil/Smix ratio of 1:9

when the water amount was less than 80% since they were isotropic and showed no birefringence under the PLM (**Figure 41a**). However, the internal droplet could be seen after the water amount reached 80% indicating the formation of coarse emulsion (**Figure 41b**). The results were in a good agreement with the results from PCS and their hazy appearance.

The system with *Z. cassumunar* oil/Smix ratio of 2:8 showed no birefringence under the PLM when the water amount was not more than 50%. Accompany with their isotropic property, they were defined as microemulsions. Liquid crystal, usually anisotropic system with the birefringence (41), was found when the water amount was 60-80% in the system with *Z. cassumunar* oil/Smix ratio of 2:8. The colourful textures of oily streaks can be seen in those samples as shown in **Figure 41c**. The results were in a good agreement with the results from PCS and their gel-like property. Moreover, the internal droplet of coarse emulsion could be seen when the water amount was 90% in the system with ZC/Smix ratio of 2:8. The results were also in a good agreement with the results from PCS and their hazy appearance.

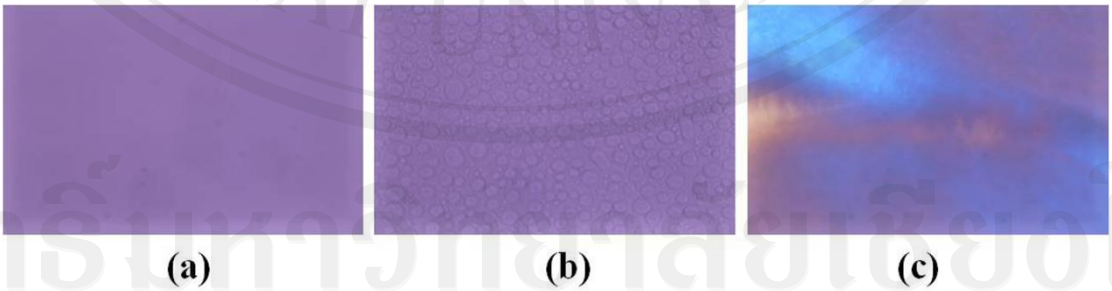

Figure 41 PLM pictures at the magnification of 100× of selected samples from microemulsion with *Z. cassumunar* oil /Smix of 1:9 and 50% of water amount (a), 90% of water amount (b) and selected samples from microemulsion with *Z. cassumunar* oil/Smix of 2:8 and 60% of water amount (c).

The thermal behaviour of water in the systems was investigated in a comparison with that of pure water by DSC as shown in **Figure 42**. Upon the cooling stage, pure water showed a large exothermic peak at -17°C which was defined as a freezing temperature and during the heating run, it showed an endothermic peak at 0°C which was defined as a melting temperature (42, 133-134).

In the system with *Z. cassumunar* oil/Smix of 1:9, the freezing exothermic peak and the melting endothermic peak were found when the water content were 70% and over. Below that water level, both freezing exotherm and melting endotherm were absent. Garti *et al*. (2000) revealed that the absence of any water freezing peak in the binary water-surfactant mixtures indicates presence of a strong water-surfactant interaction (135). Therefore, the microemulsions with less than 70% of water amount were suggested to be W/O or bicontinuous type. In addition, Boonme *et al*. (2006) stated that bulk (free) water of external phase was assumed to have similar physicochemical properties to those of pure water (42). Therefore, O/W system should show both freezing exothermic peak and melting endothermic peak at the same position of pure water. This data support our suggestion from the study of DSC that water changes from the internal pseudo phase into the external phase after 70% of water content. Accompany with the results from PCS and the physical appearance, it can be concluded the O/W microemulsion was formed when water content was 70% and O/W emulsions were formed when water content was 80% and over. However, it was noted that neither freezing exotherm nor melting endotherm occurred at the same position of pure water because of the partial miscibility of Triton X-114 and PG with water (42).

In the system with *Z. cassumunar* oil/Smix of 2:8, there is neither freezing exothermic peak nor melting endothermic peak observed in the microemulsion range (10-50% water). Therefore, all microemulsion formed was W/O type. However, the freezing exothermic peak and melting endothermic peak were found in the gel-like system (60-80% water) and coarse emulsion (90% water) in the system with *Z. cassumunar* oil/Smix of 20:80.

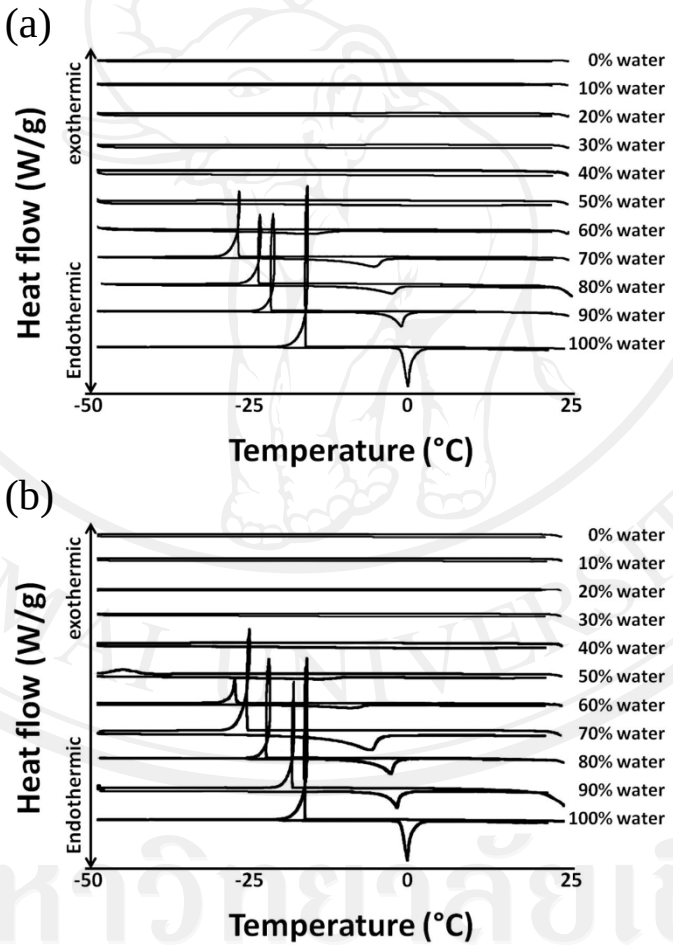

Figure 42 Differential scanning thermograms of formulations at a constant *Z. cassumunar* oil/Smix ratio of 1:9 (a) and 2:8 (b) upon increasing amount of water.

Electrical conductivity measurement has been proved to be a convenient and reliable method for probing the structure features of microemulsion system (135). A change in electrical conductivity apparently indicates a variation in the microstructure of the microemulsion (118). The conductivity of microemulsion with *Z. cassumunar* oil/Smix of 1:9 displayed a sigmoidal pattern along the increase of water fraction as shown in **Figure 43a**. With the increasing of the water amount, there must be some kind of structural transition by which W/O microemulsion inverts into O/W microemulsion (137). As long as there is no phase separation and the system remains isotropic, the inversion may be a gradual change through a bicontinuous structure (42, 137). At small water volume, the conductivity remained low. It is generally known that the W/O microemulsion can be formed at low water content and the oil is continuous. Then the conductivity sharply increased at an aqueous phase above 20% since the aqueous phase dominate the electrical conductivity of a bicontinuous microemulsion in which the conducting aqueous phase exists in a three dimensional network (108). Therefore, this sharp rising of conductivity could be referred to the transition from W/O microemulsion to bicontinuous microemulsion. After that, a sharp increase in conductivity turned to a lower increased rate at 60% of the water amount. This phenomenon was regarded as the transition from a bicontinuous microemulsion to an O/W microemulsion (47, 108). The results corresponded well with the results from DSC that the freezing exothermic peaks and melting endothermic peaks of O/W system were found when the water amount was 60% and over.

According to the system with *Z. cassumunar* oil/Smix of 2:8, the electrical conductivity was very low when the water content was lower than 15% and sharply

increased after this point (**Figure 43b**). Therefore, the structural transition from W/O to bicontinuous microemulsion occurred at this water concentration. Since there was no lower increasing rate of the conductivity within the microemulsion range, it was suggested that the bicontinuous microemulsion did not turned to O/W microemulsions. The results were in a good agreement with the results from previous data of DSC that neither freezing exothermic peak nor melting endothermic peak was observed in the microemulsion range. However, the bicontinuous microemulsion turned to the liquid crystal system after 50% of water amount. The obviously decrease of electrical conductivity was found in those gel-like formulations (data not shown) since the electrical conductivity also depends on the local viscosity or microviscosity around the charge carriers (138).

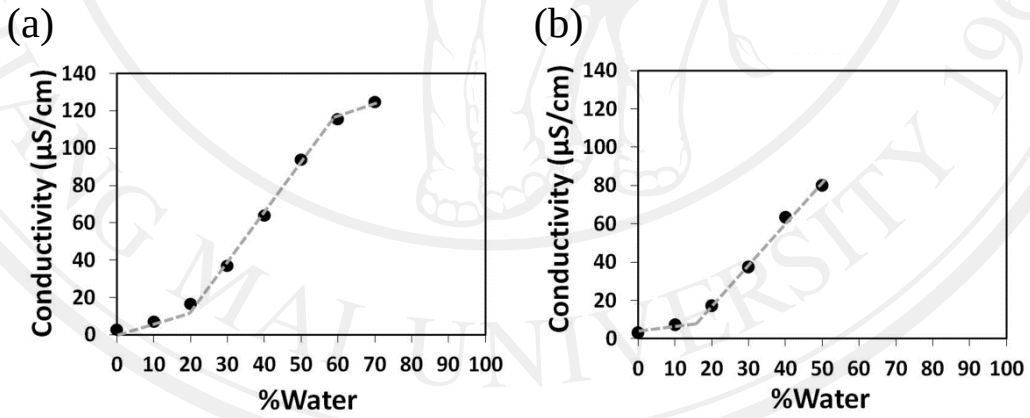

Figure 43 Electrical conductivity versus aqueous phase amount (%) of microemulsions with *Z. cassumunar* oil/Smix of 1:9 (a) and 2:8 (b).

The results of rheological measurement of each microemulsion are shown in **Figure 44**. All formulations acted as Newtonian fluid which stress versus strain rate curve is linear and passes through the origin (41, 47). The viscosity was calculated

using constant of proportionality as shown in the following equation; $\tau = \mu(du/dy)$, when τ is the shear stress (Pa), μ is the viscosity and du/dy is the velocity gradient perpendicular to the direction of shear or strain rate (s^{-1}) (139-140). The Newtonian flow behavior accompany with the low viscosity of these one phase systems confirmed the formation of microemulsions (141). Moreover, Burghardt *et al*. (2002) revealed that bicontinuous microemulsion also displayed linear viscoelastic properties (142). The viscosity of microemulsion with *Z. cassumunar* oil/Smix of 1:9 remained stable when the water fraction was less than 60% and then it distinctly decreased. The decreased viscosity indicated the change to O/W microemulsions which was consistent well with the DSC and conductivity data reported above. A decrease in viscosity at higher water concentrations of O/W microemulsions is explained by the dilution effect of additional water added to external phase of the system (42). Regard to microemulsions with *Z. cassumunar* oil/Smix of 2:8, the viscosity remained stable with no obvious decrease. This result corresponds well with the study of DSC and conductivity.

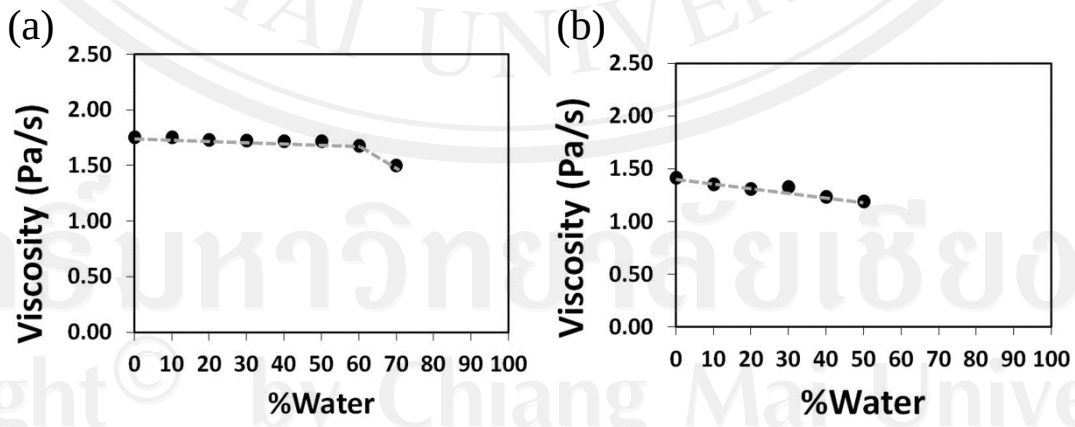

Figure 44 Viscosity versus aqueous phase amount (%) of microemulsions with *Z. cassumunar* oil/Smix of 1:9 (a) and 2:8 (b).

After the study of phase diagram of *C. citratus* oil and *Z. cassumunar* oil, six phase diagrams which their compositions are shown in **Table 15** were selected for the comparative characterizations. PG or ethanol was selected to be a co-surfactant since they gave a large microemulsion region in the previous studies. Moreover, both PG and ethanol were able to be good penetration enhancers. Ethanol is commonly used in many transdermal formulations since it can exert its permeation enhancing activity through various mechanisms. Firstly, ethanol acts as a solvent to increase the solubility of the drug (103). Further, permeation of ethanol into the stratum corneum alters the solubility properties of the tissue with a consequent improvement for drug partitioning into the membrane (143). Additionally, the rapid permeation of ethanol or evaporative loss of this volatile solvent increases drug concentration beyond saturated solubility providing a supersaturated state with a greater driving force for permeation (103). Moreover, the rapid permeation across the skin of ethanol cause the "solvent drag" which the permeant was carried into the tissue as ethanol traverses (144). PG is also widely used in dermatological preparations since it was reported to increase the permeation of many drugs (130). Because PG permeates well through human stratum corneum, it alters thermodynamic activity of the drug in the vehicle which would in turn modify the driving force for diffusion, PG which partition into the tissue facilitates uptake of the drug into skin and there may be some minor disturbance to intercellular lipid packing within the stratum corneum bilayers (103).

Table 15 Compositions of microemulsion systems.

System	Oil	Surfactant	Co-surfactant	Water
I	*Z. cassumunar* oil	Tween 20	PG	Water
II	*Z. cassumunar* oil	Tween 20	Ethanol	Water
III	*Z. cassumunar* oil	Triton X-114	PG	Water
IV	*Z. cassumunar* oil	Triton X-114	Ethanol	Water
V	*C. citratus* oil	Tween 20	Ethanol	Water
VI	*C. citratus* oil	Triton X-114	Ethanol	Water

The selected microemulsions were composed of oil: Smix: water in the ratio of 1:5:4 and 2:5:3. The electrical conductivity of each formulation is shown in **Figure 45**. The results indicated the higher electrical conductivity of systems containing higher amount of water. To see the effect of surfactant type on the electrical conductivity, formulation I and III, II and IV, as well as V and VI were compared. The results showed that microemulsion using Tween 20 as a surfactant exhibited higher electrical conductivity than that of Triton X-114. The reason was from the higher HLB value of Tween 20 which made the easier formation of O/W microemulsions (111-112). The effect of co-surfactant type can be seen when compare formulation I with II and III with IV. The electrical conductivity of the PG containing microemulsion was lower than that of the ethanol containing microemulsion at the same Smix/oil ratios although the water is strongly bound to both ethanol and PG (140).

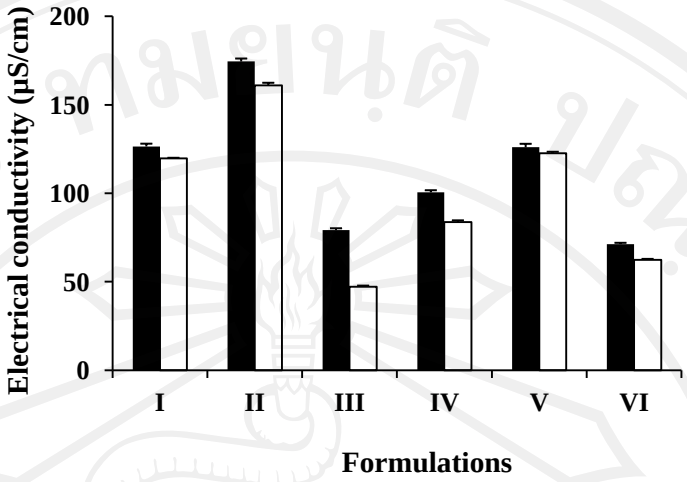

Figure 45 Electrical conductivity of microemulsions systems containing oil : Smix : water in the ratio of 1:5:4 (■) and 2:5:3 (□).

Viscosity of each formulation was investigated by bob-and-cup viscometer. All of formulations shows Newtonian flow behavior with low viscosities (range from 28.2 to 35.9 Pa·s) which are represented to a typical characteristic of microemulsion. Rheogram of microemulsion as shown in **Figure 46** indicates the Newtonian flow behavior which stress versus strain rate curve is linear and passes through the origin (41).

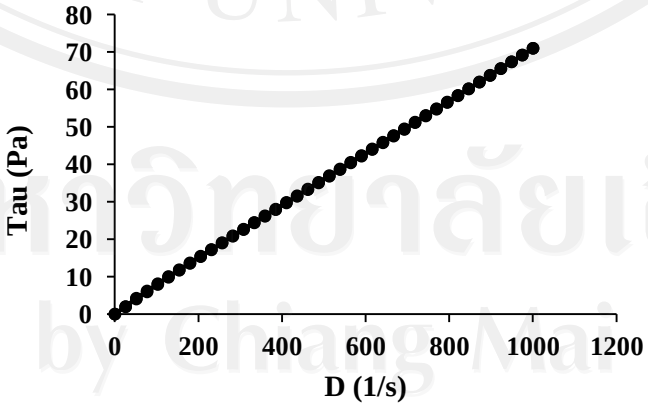

Figure 46 Rheogram of microemulsion system containing 10% *Z. cassumunar* oil/Triton X-114/ethanol/water when Triton X-114/ethanol ratio was 2:1.

Transdermal preparation with smaller internal droplet was more effective compared with the larger one (145). The percutaneous permeation increase since the smaller droplets have better chance to adhere to membranes and to transport bioactive molecules in a more controlled fashion (35, 146). Therefore, the diameter of the internal droplet size of microemulsions was determined by using light scattering measurements. The formulation with smaller internal droplet was selected for the further in depth study. Various factors affecting the internal droplet size were studied to select the most suitable components of the microemulsions. Since microemulsions are quaternary systems composing of oil, surfactant, co-surfactant and water, the factors enrolled in this study were type of oil, surfactant and co-surfactant. The results as can be seen in **Figure 47** show that microemulsions containing *Z. cassumunar* oil have smaller internal droplet sizes than that of *C. citratus* oil. Moreover, the effect of surfactant type on the size of internal droplet was also obviously that microemulsions containing Triton X-114 exhibited the smaller droplet size than that of Tween 20 (**Figure 48**). In addition, different type of co-surfactant also affected the particle size of microemulsions, the results as shown in **Figure 49** indicates that microemulsions containing ethanol have smaller droplet size than that of PG. Therefore, the most suitable microemulsion system composed of *Z. cassumunar* oil, Triton X-114, ethanol and water was selected for the incorporation of TD alkaloidal extract.

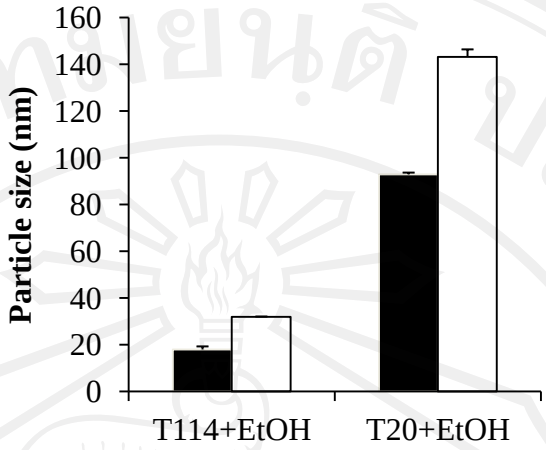

Figure 47 Internal droplet sizes of microemulsions containing *Z. cassumunar* oil (■) and *C. citratus* oil (□) when ethanol (EtOH) was used as a co-sufactant and Triton X-114 (T114) or Tween 20 (T20) was used as a surfactant. The oil:Smix:water was 2:5:3 when Smix was surfactant to co-surfactant in the ratio of 2:1.

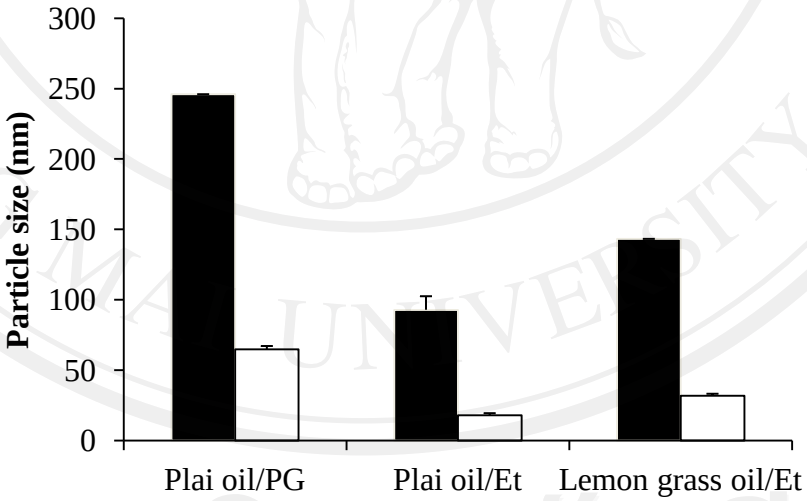

Figure 48 Internal droplet sizes of microemulsions containing Tween 20 (■) and Triton X-114 (□) when PG or ethanol (Et) was used as a co-surfactant and the oil phase was *Z. cassumunar* oil (Plai oil) or *C. citratus* oil (Lemon grass oil). The oil:Smix:water was 2:5:3 when Smix was surfactant to co-surfactant in the ratio of 2:1.

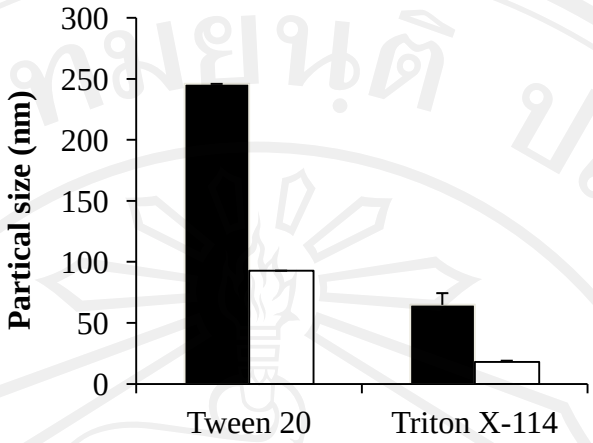

Figure 49 Internal droplet sizes of microemulsions containing PG (■) and ethanol (□) when Tween 20 or Triton X-114 was used as a surfactant and the oil phase was *Z. cassumunar* oil. The oil:Smix:water was 2:5:3 when Smix was surfactant to co-surfactant in the ratio of 2:1.

The TD alkaloidal extract was incorporated into the selected microemulsions, the positions in phase diagram are shown in **Figure 50**. Different amounts of TD alkaloidal extracted range from 0.05 to 5.00 mg/mL. The droplet size of microemulsion containing higher amount of the extract was larger than that of smaller one as shown in **Figure 51**. This is an evidence to indicate that TD alkaloidal extract was entrapped inside the internal droplet of microemulsion. However, the further microstructure characterizations are needed for the confirmation of this primary hypothesis since the microstructure is directly related to the efficient use in many scientific and industrial applications (147).

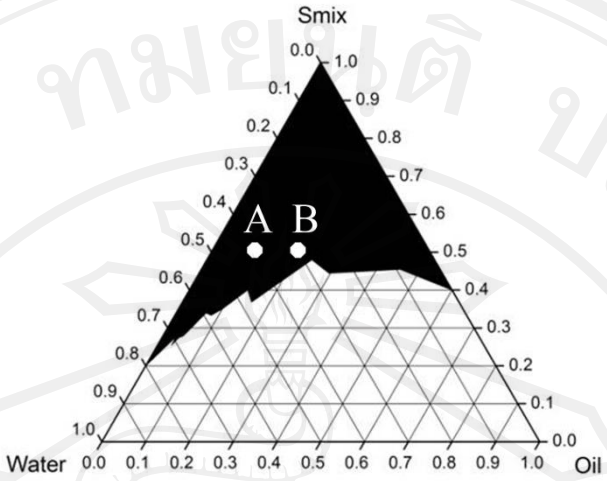

Figure 50 Pseudoternary phase diagram of *Z. cassumunar* oil/Triton X-114/ethanol/water. The dark area represents the region of microemulsion. A and B are the selected microemulsions containing oil:Smix:water in the ratio of 1:5:4 and 2:5:3, respectively.

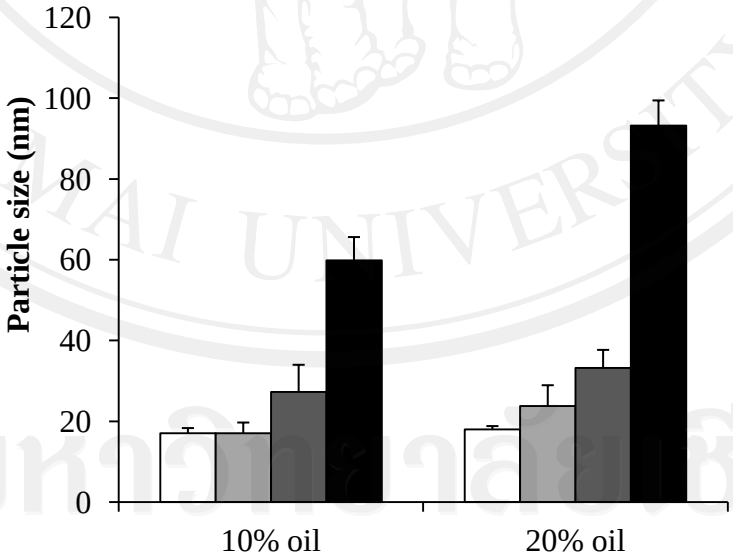

Figure 51 Internal droplet sizes of *Z. cassumunar* oil/Triton X-114/ethanol/water microemulsion (□), microemulsion containing TD alkaloidal extract: 0.05 mg/mL (■), 0.50 mg/mL (■) and 5.00 mg/mL (■). The ratio of Triton X-114/ethanol was 2:1.

To evaluate the further microstructures, 5 mg/mL of TD alkaloidal extract was incorporated into the 10 formulations along dilution line A and 10 formulations along dilution line B as shown in **Figure 52**. According to the dilution line A, clear yellowish liquids, which were expected to be microemulsion, were found in A1 to A7. However, the jelly-like formulations (A8 and A9) were observed when a water amount over 60%. Furthermore, coarse emulsion was formed when the water amount was increased to 90%. The clear yellowish liquids were also found in formulation B1 to B5 along the dilution line B. However, the jelly-liked formulations (B6-B9) were formed when the water amount over 40% and the coarse emulsion (B10) was formed when the water amount was 90%.

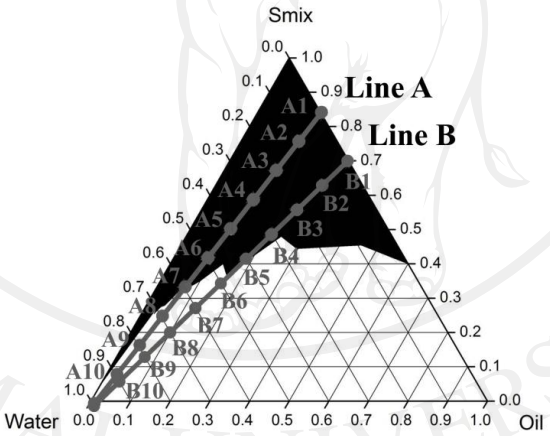

Figure 52 Pseudoternary phase diagram of *Z. cassumunar* oil/Triton X-114/ethanol/water system. The dark area represented to the microemulsion region. The dilution line A and B were composed of oil:Smix in the ratio of 1:5 and 2:5, respectively.

Rheological behavior and viscosity is a characteristic property of any fluid (137). In microemulsion systems, viscosity was low, acted as Newtonian fluid and remained constant at any shear rates (41). The Newtonian flow behavior, which was

found in formulations with the water amount lower than 60% along dilution line A (A1-A7) and 40% along dilution line B (B1-B5), indicated that they were micromulsions. These results coincided well with their physical appearance of clear liquid. On the other hand, the formulations with jelly-liked property showed a pseudoplastic flow patterns. The relations between the viscosity and the amount of aqueous phase were shown in **Figure 53**. Low viscosity was detected in the microemulsion systems (A1-A7 and B1-B5). Microemulsions along the dilution line B which contained 28.5% of *Z. cassumunar* oil in non-aqueous phase exhibited about double viscosity of that of line A which contained only 16.6% of the oil in non-aqueous phase. It was obvious that the viscosity significantly increased when a microemulsion contained higher amount of oil. With more water volume, no change in viscosity of microemulsion was observed but an extreme increase in viscosity was found in the formulations with jelly-like appearance. After that, a decrease in viscosity at higher water concentrations is explained by the dilution effect of additional water added to the system (148).

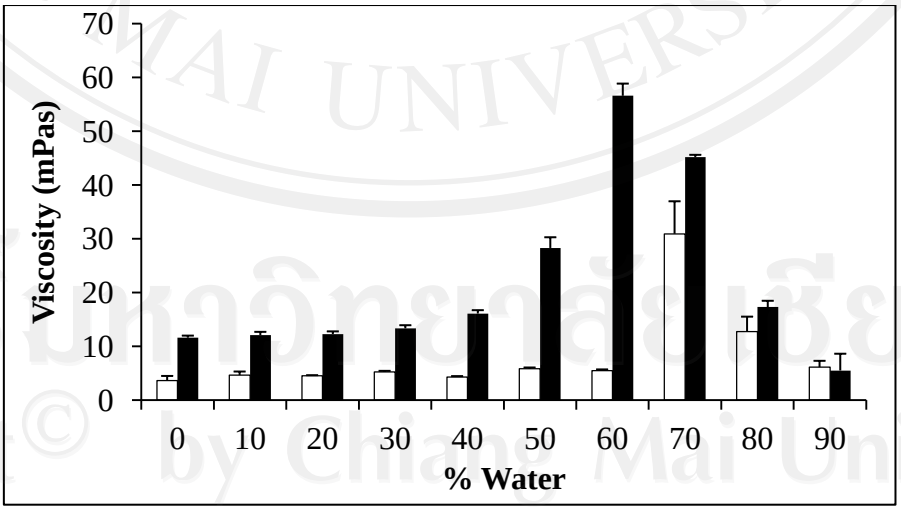

Figure 53 The relationship between viscosity of formulations along the dilution line (A:□ , B:■) and percentage of water amount in the formulations.

To distinguish liquid crystals from microemulsions, PLM was used to investigate the birefringence which is commonly found only in the system with liquid crystals (132). The darkness under the cross-PLM (**Figure 54a**) which was indicated as no birefringence and therefore classified as isotropic dispersion of spherical droplets were found in all formulations which were seen as clear yellowish liquids including A1-A7 and B1-B5. These findings leaded to assumption of spherical micelles or microemulsions of these formulations (42). On the other hand, the liquid crystal which was seen as colourful textures under the cross-PLM was observed in the jelly-liked formulations (A8-A9 and B6-B9). The liquid crystals are usually anisotropic of lamellar areas, oily streaks, fan structures, batonnets and Maltese crosses (41). In our study, the jelly-like formulations were anisotropic of lamellar liquid showing Maltese crosses (**Figure 54b**) and oily streaks (**Figure 54c** and **54d**). Moreover, the liquid crystals in water were found in turbid jelly-liked formulations (B7-B9) (**Figure 54e**). Formulation A10 and B10 which were coarse emulsion showed no birefringence but internal droplets could be seen under the cross-PLM with the magnification of 40× (**Figure 54f**). The results from PLM of these samples were in a good agreement with their viscosity. All formulations with low viscosity were isotropic while the formulations with higher viscosity were anisotropic. Since other than the birefringence observed under the cross-polarized light microscopy, microemulsions and liquid crystals have unique properties e.g. low viscosity in microemulsions but higher viscosity in liquid crystals (139).

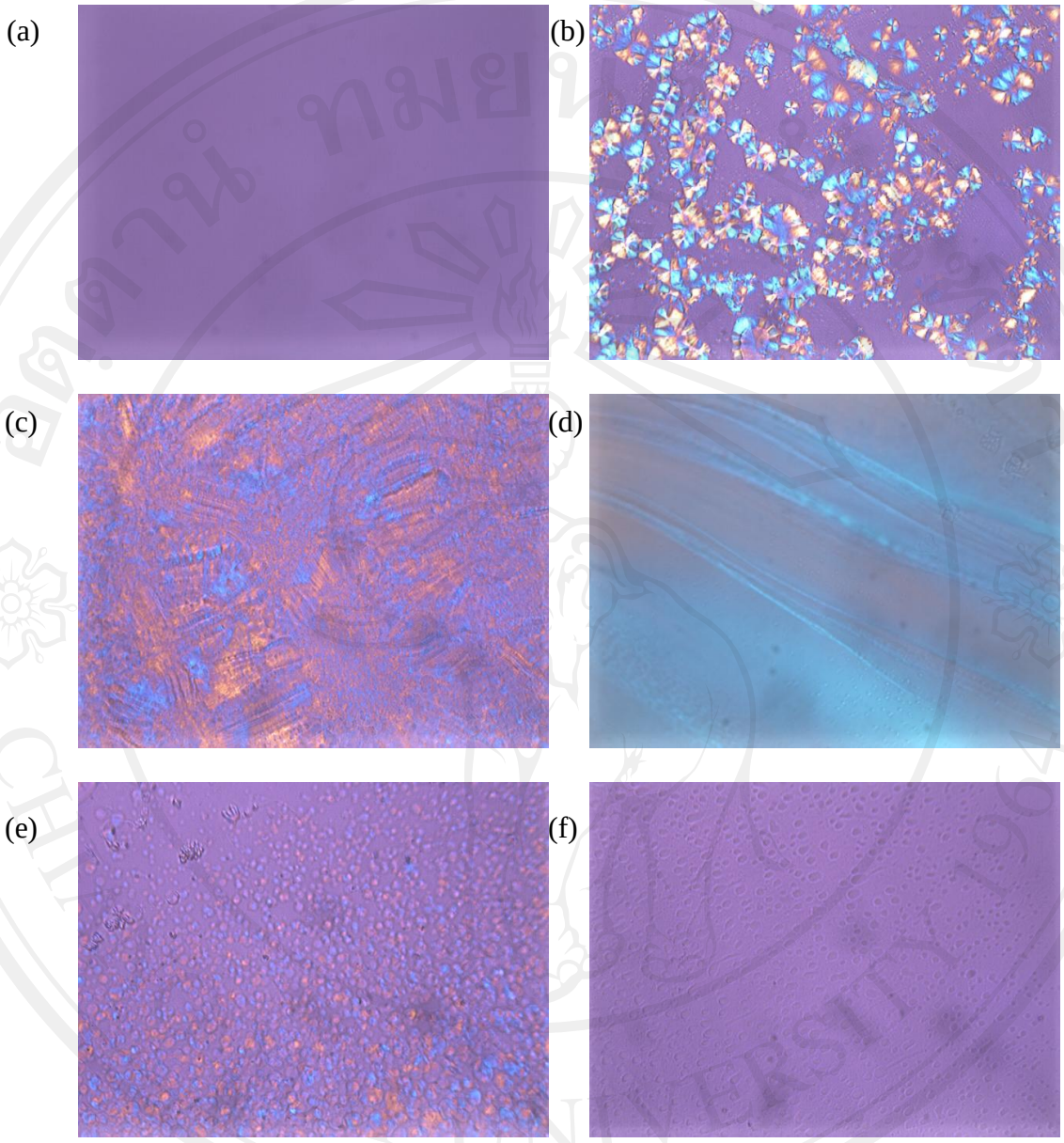

Figure 54 PLM picture of isotropic formulation (magnification 40×) which was found in formulation A1-A7 and B1-B5 (a), anisotropic formulation with Maltese crosses (magnification 40×) which was found in formulation B6 (b), anisotropic formulation with oily streaks (magnification 40×) which was found in formulation A8 and A9 (c and d), anisotropic of liquid crystal in water (magnification 40×) which was found in formulation B7-B9 (e) and coarse emulsion (magnification 40×) which was found in formulation A10 and B10 (f).

Electrical conductivity measurement is frequently used to investigate structural changes in micoremulsion systems (119-120) since it has been proved to be a convenient and reliable method for probing the structure features of emulsion and micoremulsion (29). Moreover, the presence of electrolyte in a nonionic microemulsion is necessary to provide ions for a charge transport (139), 0.1 M NaCl was therefore used as an aqueous phase instead of distilled water. A relationship between conductivity and % water is shown in **Figure 55**. Along the dilution lines, the conductivity is initially very low in the oil-Smix mixture but linearly increases as more aqueous phase is added. The changes in conductivity along the dilution line were not perspicuous until the jelly-liked formulations were formed. The obviously decrease of electrical conductivity was found in those jelly-liked formulations since the electrical conductivity also depends on the local viscosity or microviscosity around the charge carriers (138).

The microemulsions with alkaloidal extract exhibit higher electrical conductivity because of the free electron of amine in indole alkaloid (30). However, both microemulsions with and without the alkaloidal extract showed the unclear changing point to indicate the type microemulsions whether they are O/W, bicontinuous or W/O. Our previous study indicated the substantially increase in electrical conductivity of water/*C.citratus* oil/Tween 20/ethanol system as a transition point from a W/O to an O/W microemulsion (45). Kogan *et al*. (2009) also reported the exponential increase of electrical conductivity in triacetin/D-R-tocopherol acetate/ethanol/Tween 60 system as the water content increases and the transitions from a W/O to a bicontinuous and a bicontinuous to an O/W microemulsion were identified (149). Nevertheless, the exponential trend and the substantially increase

was not found in our system in the present study. Therefore, the microemulsions might be all W/O droplet type and more investigations were needed.

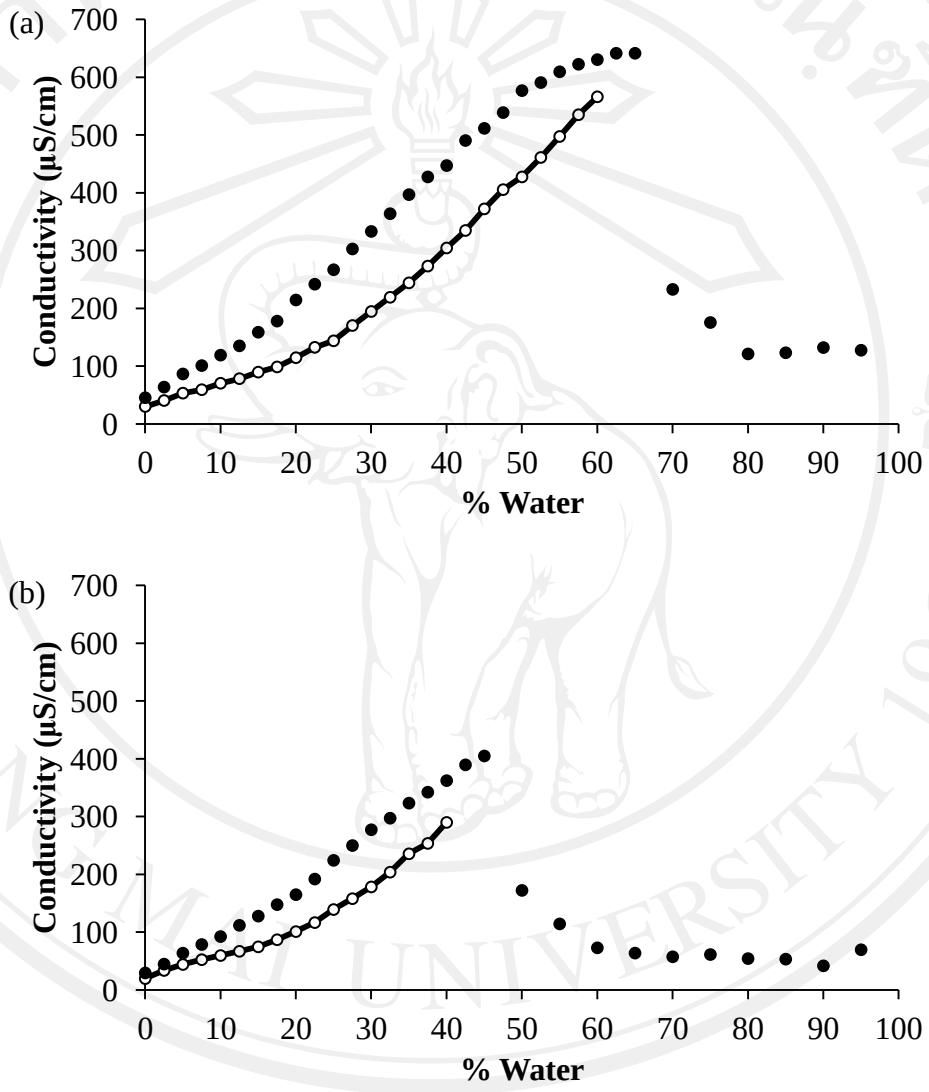

Figure 55 Electrical conductivity of formulations with TD alkaloidal extract (●) and without TD alkaloidal extract (○) along line A (a) and line B (b) with increasing water.

Investigating water thermal behaviour is a fast helpful method to understand the microstructure of microemulsions (150). The thermal behaviour of water in the

formulations was investigated in a comparison with that of pure water by DSC as shown in **Figure 56**. Upon the cooling stage, the pure water showed a large exotherm at -17°C which was defined as a freezing temperature of a supercooled water (138-139). Along dilution line A, the freezing exotherm was absent until the water amount reached 50%. After the water amount increased to 50%, the exotherm became apparent in the cooling curve around -30°C and the peak amplitude increased with larger water content. No samples showed a freezing exotherm at the same position as the pure water because of the partial miscibility of surfactant and co-surfactant (139, 151). In the same way, the freezing exotherm was absent until the water amount reached 50% along the dilution line B. It can be assumed that water changes from the internal pseudo phase into bicontinuous phase or the external pseudo phase of the microemulsions at these points. Zhang and Michniak-Kohn (2011) reported that the water freezing peaks were shown in both microemulsion sample of bicontinuous and O/W microstructure (152) while Boonme *et al*. (2006) reported that the water freezing peaks were shown when the water changed from internal pseudo phase into the external pseudo phase (42). Therefore, A6 and A7 which exhibited the freezing exotherm of water can be assumed to be bicontinuous microemulsions. A8-A9 and B6-B9 which were liquid crystal also exhibited those freezing exotherm since the structure of both bicontinuous microemulsions and lamellar liquid crystals were layered geometry with elongated channels that consist of surfactant, co-surfactant and oil mixture along with a continuous water phase (149). However, Podlogar *et al*. (2004) indicated that it was hard to detect the transition to O/W type of microemulsion by DSC where the amount of surfactant was high (151).

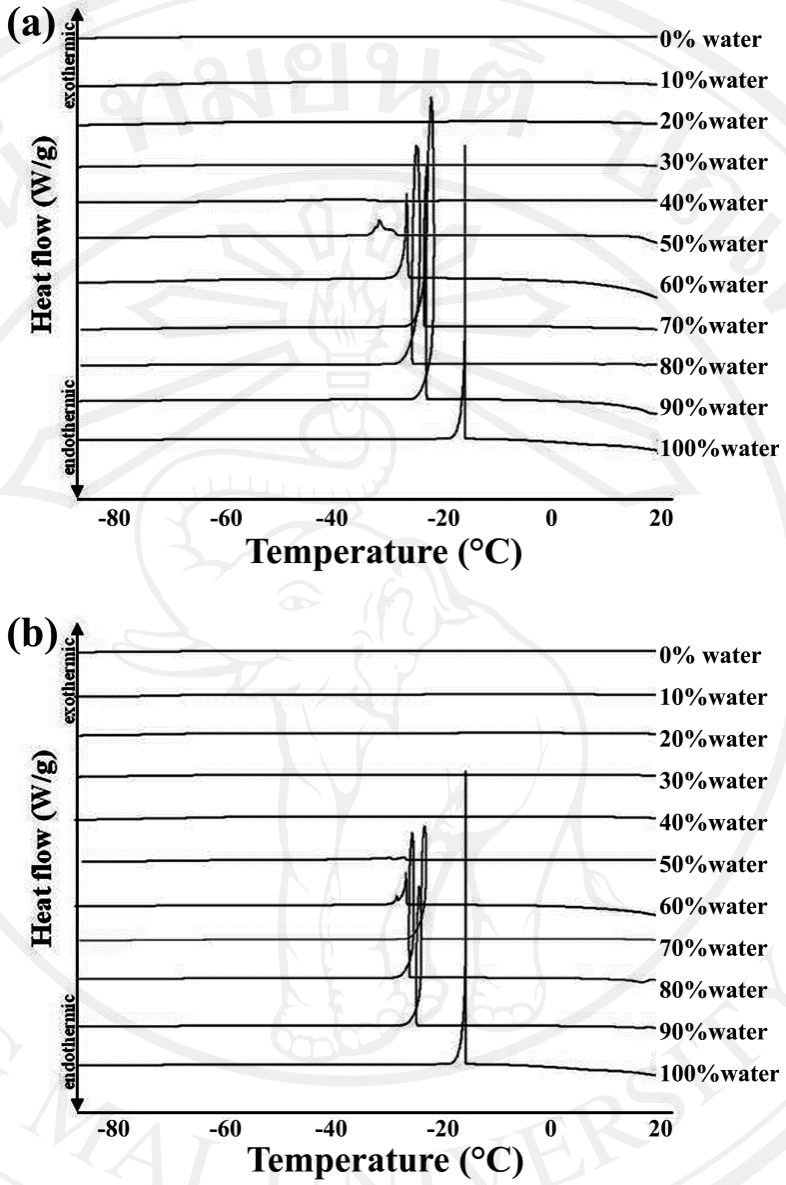

Figure 56 DSC thermogram of formulation along dilution line A (a) and dilution line B (b).

FF-TEM has been used to study a pseudoternary *Z. cassumunar*/Triton X-114/ethanol/water system varying in water concentration. A2, A4 and A6 were defined as droplet type microemulsions by FF-TEM micrographs. The reverse micelle filled with water was observed in A2 (**Figure 57a**). Those reverse micelles were then

swollen according to an adding amount of water. More and bigger reverse micelles were therefore formed in A4 and A6 (**Figure 57b** and **57c**). These results were in a good agreement with their electrical conductivity which showed that all microemulsions along the dilution line A were W/O microemulsions. However, the DSC freezing exotherms of water were found in A6 and A7 which indicated the external pseudo phase of water. Those freezing exotherms might occurred because of the freezing out of water according to the swollen reverse micelles were so large. With a further increase of the water content to 70% in A8, numerous larger water channels were clearly observed (**Figure 57d**). The FF-TEM results accompanied with the PLM are able to indicate the mixture of liquid crystal and bicontinuous microemulsion of this formulation. However, the liquid crystal alone was found in another dilution line which contained 28.5% of *Z. cassumunar* oil in non-aqueous phase because a classical flat bilayer was formed at this point (153). **Figure 57e** shows the planar lamella phase of B6 which were regularly stacked. Furthermore, the sponge-shaped system of branched bicontinuous tube existed when the water content further increased up to 90% in A10. The FF-TEM micrograph of the sponge-likes structure was shown in **Figure 57f**. The results were in a good agreement with the previous report of Zapf *et al.* that the distinct properties among micellar, bilayer and sponge-liked phase were that the micellar and sponge-liked phase were optically isotropic while the bilayer phase was birefringence (153). Finally, types of each formulation were concluded in **Table 16**.

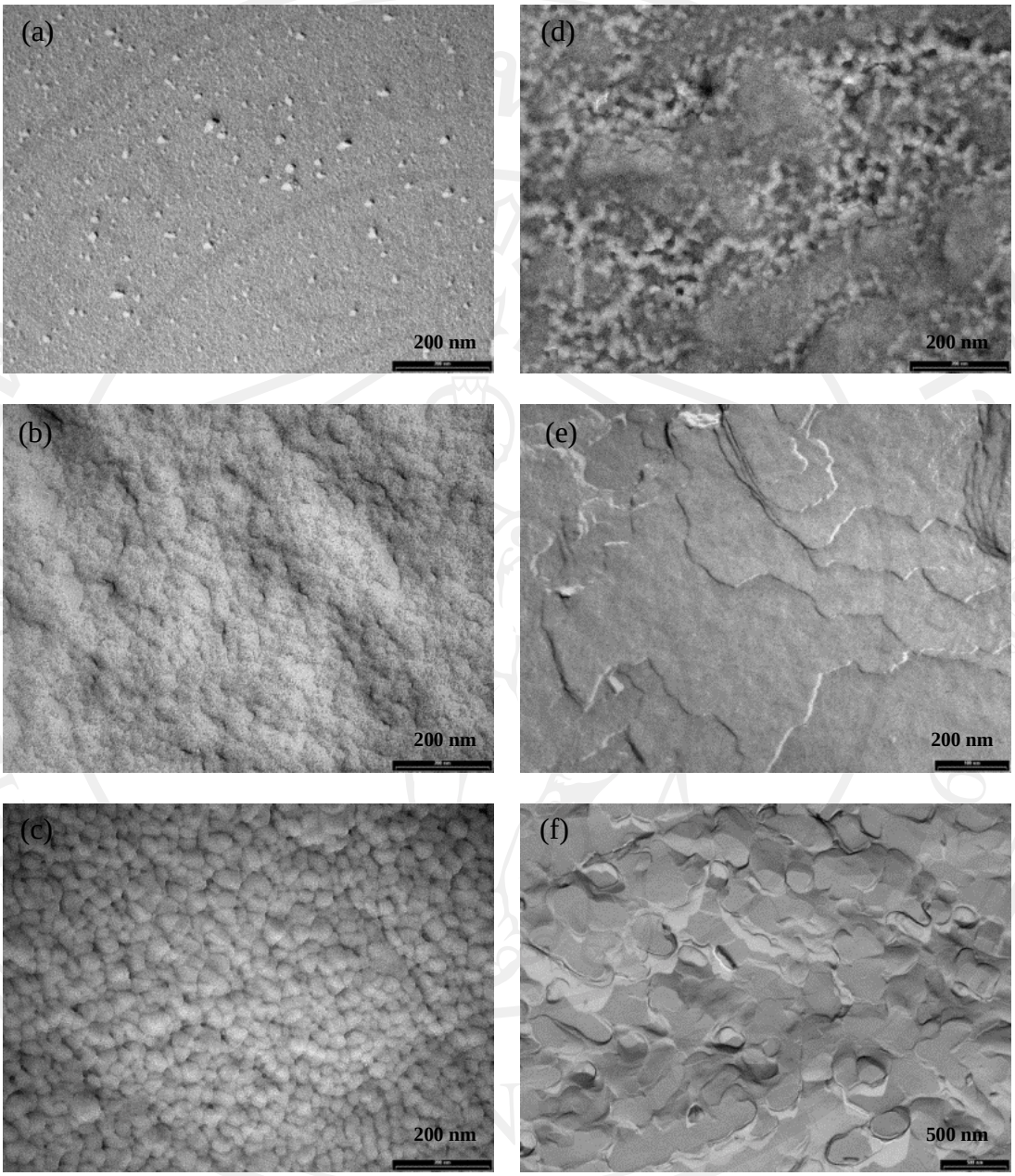

Figure 57 FF-TEM micrographs of droplet type microemulsions: A2 (a), A4 (b), A6 (c), liquid crystal in microemulsion: A8 (d), liquid crystal: B6 (e) and coarse O/W emulsion: A10 (f).

Table 16 Types of formulation from *Z. cassumunar* oil/ Triton X-114/ethanol/water systems along dilution line A and dilution line B.

% Water	Types of formulations			
	Dilution line A		Dilution line B	
0	A1	Mixture of oil and Smix	B1	Mixture of oil and Smix
10	A2	W/O microemulsion	B2	W/O microemulsion
20	A3	W/O microemulsion	B3	W/O microemulsion
30	A4	W/O microemulsion	B4	W/O microemulsion
40	A5	W/O microemulsion	B5	W/O microemulsion
50	A6	W/O microemulsion	B6	Liquid crystal
60	A7	W/O microemulsion	B7	Liquid crystal
70	A8	Liquid crystal in microemulsion	B8	Liquid crystal
80	A9	Liquid crystal in microemulsion	B9	Liquid crystal
90	A10	Coarse emulsion	B10	Coarse emulsion

Two formulations of W/O microemulsion composing of 16.6% *Z. cassumunar* oil in non-aqueous phase (A4 and A6), a formulation of W/O microemulsion composing of 16.6% *Z. cassumunar* oil in non-aqueous phase (B4), a formulation of liquid crystal in microemulsion (A8) and a formulation of liquid crystal (B6) were selected for the further stability study, *in vitro* anticholinesterase activity and *in vitro* permeation study.

AChE inhibitions of each formulation are shown in **Figure 58**. The inhibitory activities were in a range of 92.06% to 94.83% when a concentration of TD alkaloidal extract in the formulation was 10 µg/mL. They were not statistically different from

each other at this concentration because of the maximum inhibitions were reached. After each formulation was diluted to 1 µg/mL, there was still no statistically difference detected. But when the formulations were further diluted to 0.1 µg/mL, microemulsion-A4, microemulsion-A6 and liquid crystal in microemulsion-A8 were found to possess higher inhibitory activity against AChE than that of TD alkaloidal extract in PG. The reasons might be from a higher ratio of Smix to oil in formulation As (5:1) when compared with that of formulation Bs (5:2). Since the higher amount of surfactant caused higher solubility. Therefore, it leads to more attachment of the alkaloids with the enzyme.

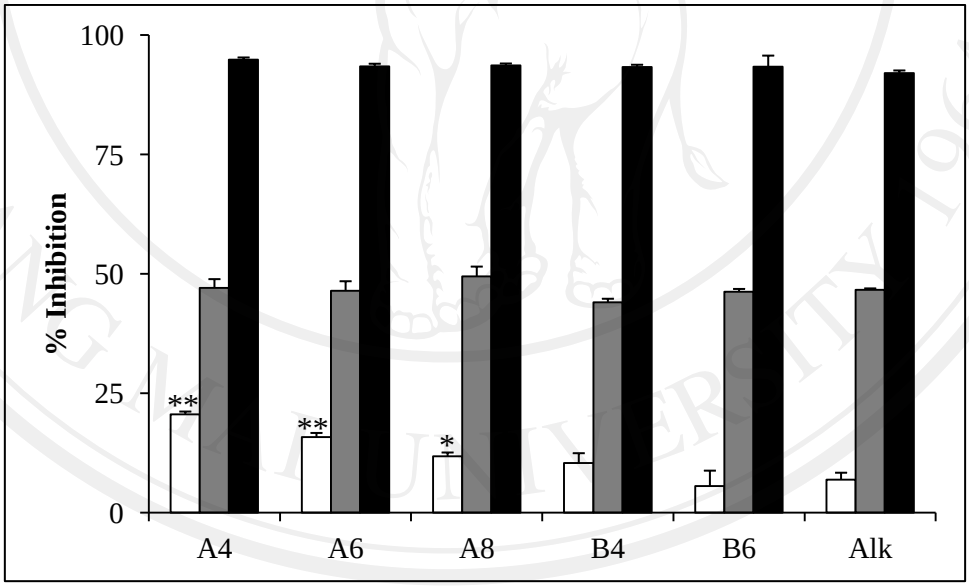

Figure 58 Inhibitory activity against AChE of microemulsion-A4, microemulsion-A6, liquid crystal in microemulsion-A8, microemulsion-B4, liquid crystal-B6 and TD alkaloidal extract in PG (Alk) when the concentration of TD alkaloidal extract in each formulation was 0.1 (□), 1 (■) and 10 µg/mL (■) (** = $p < 0.001$ and * = $p < 0.05$ when compared with Alk).

The inhibitory activity against AChE of each formulation was then followed up for 180 days after they were stored in 4°C, 30°C and 45°C. The results as shown in **Figure 59a** indicated the lost of inhibitory activity when TD alkaloidal extract in PG was stored in 45°C. The final inhibitory activity was 61.39±2.80% of the original inhibitory activity in this high temperature. The results were in a good agreement with the previous study of stability of TD alkaloidal extract in part II that the amount of TD alkaloidal extract gradually decreased to 60% after 6-month storage in 45°C. Therefore, the decrease of inhibitory activity was related well with the depletion of the TD alkaloidal extract amount which was measured from the amount of 3'-*R/S*-hydroxyvoacamine by HPLC. Moreover, darker color of TD alkaloidal extract in PG was detected in the formulations stored at 45°C since day 60 as shown in **Figure 60**. The inhibitory activity of TD alkaloidal extract in PG was also gradually decreased to 77.48±0.34% and 79.55±1.15% when they were kept at 4°C and 30°C, respectively. The reasons might be from the oxidation of some compounds when exposure to light and oxygen. The light protected container and nitrogen purge which were recommended from the previous stability study was not used in this part in order to highlight the protection property of the microemulsion on the alkaloidal extract. The TD alkaloidal extract encapsulated in microemulsion possess higher inhibitory activity after stored in various temperatures for 180 days. Moreover, the results indicated that high temperature of the storage had no effect on the inhibitory activity of all microemulsions as shown in **Figure 59d, 59e** and **59f**. The final inhibitory activity of A4, A6 and B4 were 86.71±2.52%, 81.14±2.03 and 82.78±2.63, respectively, which were higher than that of TD alkaloidal extract in PG. The final inhibitory activity of liquid crystal in microemulsion-A8 and liquid crystal-B6 were

also higher than that of TD alkaloidal extract in PG. Their final inhibitory activities were 83.84±2.11% and 82.15±1.92%, respectively. However, the substantial differences in inhibitory activity between storage in 45°C and the others temperatures were detected in the beginning because of the conformation changes in the poly(oxyethylene) chain of Triton X-114 by high temperature (154).

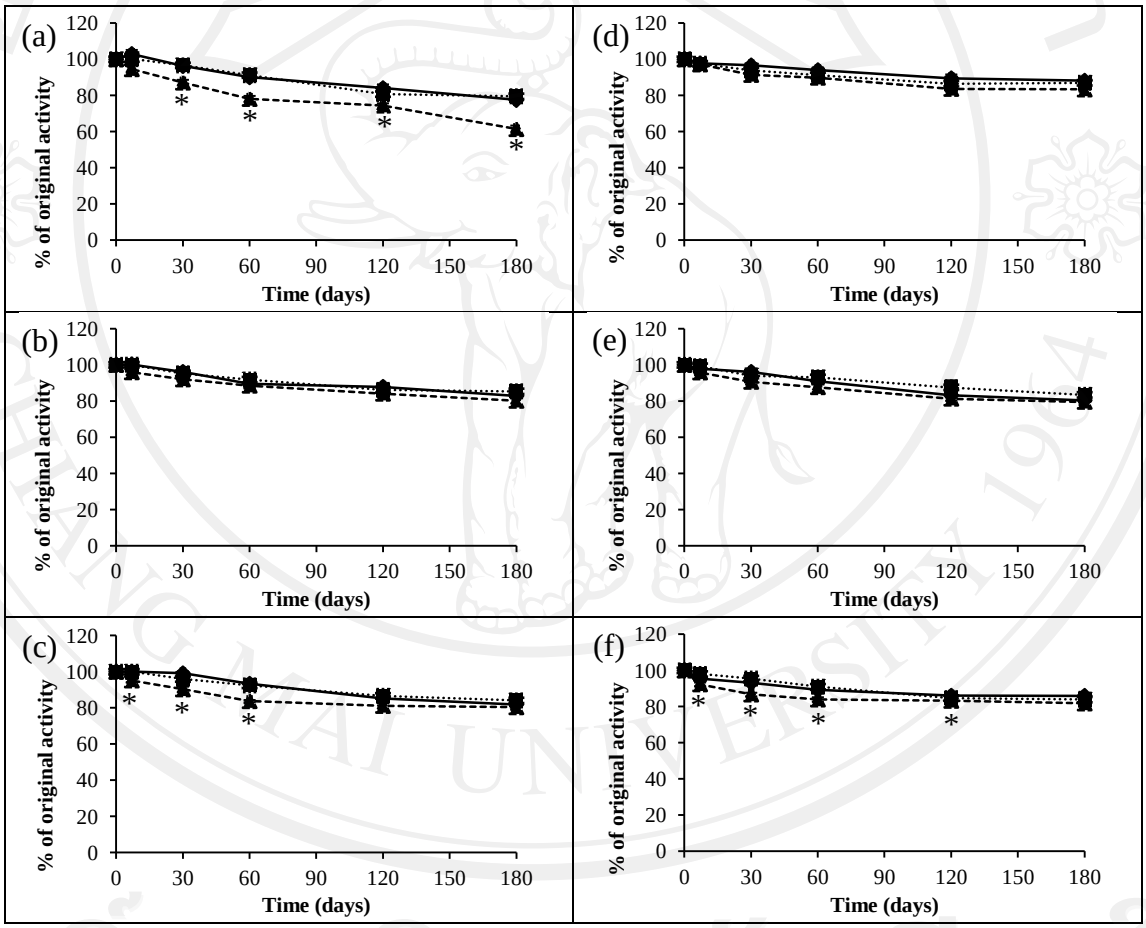

Figure 59 Graph of stability of TD alkaloidal extract in PG (a), microemulsion-B4 (b), liquid crystal-B6 (c), microemulsion-A4 (d), microemulsion-A6 (e) and liquid crystal in microemulsion-A8 (f) when each formulation was kept in 4°C (—●—), 30°C (···■···) and 45°C (- -▲- -) for 180 days ($p < 0.05$).

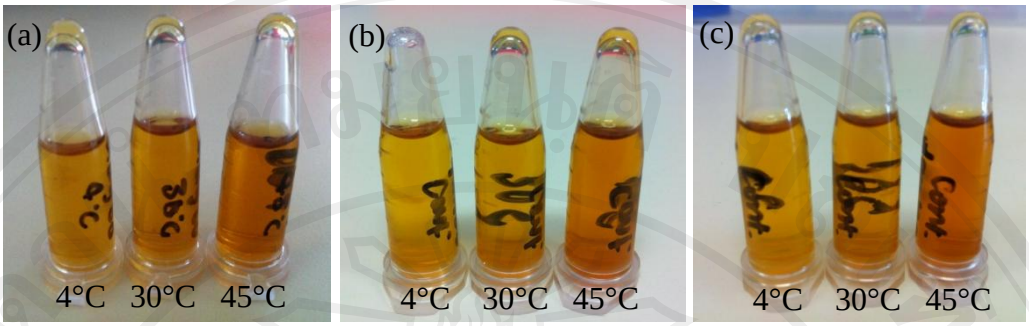

Figure 60 Physical appearances of TD alkaloidal extract in PG which were stored in various temperatures for 60 (a), 120 (b) and 180 days (c).

The cumulative release of each formulation are shown in **Figure 61.** Within 24 hr, there was no TD alkaloidal extract detected in the receptor media of franz cell treated with the TD alkaloidal extract in PG. Although PG is widely used as a penetration enhancer in topical dermatological preparations, either alone or in combination with other penetration enhancers (130,155-156), it did not assist the permeation of the TD alkaloidal extract through the skin in this study. Since the penetration enhancer effect of PG is most noticeable when it was used in the *in-vivo* mimic situation (where the stratum corneum is not fully hydrated) either on its own or when operating synergistically with other accelerants (157). The activity of PG is thought to result from solvation of alpha-keratin within the stratum corneum where proteinaceous hydrogen bonding sites occupied, results in reducing of drug-tissue binding and thus promoting permeation (155). Therefore, PG did not increase the permeation when applied to fully hydrated tissue because the PG does not influence horny layer lipid structure (157). Most of TD alkaloidal extract could not consequently penetrate through the skin and retained on the skin. Only small amount of the alkaloidal extract can be detected in the skin as shown in **Figure 62.**

On another hand, the TD alkaloidal extract was detected from the receptor media of franz cells that were treated with various systems of *Z. cassumunar* oil/TritonX-114/ethanol/water. Both microemulsions and liquid crystalline systems show an enhancing effect on skin permeation of the TD alkaloidal extract. Since the microstructure of the microemulsion and the arrangement of the components in the liquid crystal systems can create a very small droplet size and very low interfacial tension that leads to the very large surface area for drug transfer to skin (158). The cumulative amount of the TD alkaloidal extract per unit area of skin that has passed through the skin after 24 hr (Q_{24}) of A4, A6, A8, B4 and B6 were shown in **Table 17**.

Table 17 The cumulative amount of the TD alkaloidal extract per unit area of skin that has passed through the skin after 24 hr (Q_{24}).

Formulation	Q_{24} (μg/cm^2)
A4	0.22±0.12
A6	0.11±0.06
A8	0.10±0.07
B4	0.37±0.20
B6	0.54±0.28

B6 which was liquid crystal showed the greatest Q_{24} when B4 which was microemulsion came in the second place. The formulations containing 16.6% of *Z. cassumunar* oil in non-aqueous phase possessed lower Q_{24} than that of the formulations containing 28.5% of the oil. These results were in a good agreement with the results from skin retention as shown in **Figure 62.** The results indicate that

B4 and B6 possess higher skin retention of the alkaloidal extract than that of A4, A6 and A8. It also means that higher amount of the alkaloidal extract from B6 can partition into the skin which brings about to the highest Q_{24}. The interlamelarlly fixed water, presented in lamellar liquid crystalline phases of B6, may serve as a formulation reservoir for controlled skin hydration which leads to the prolongation of skin hydration and contribute to the penetration enhancing effect (159). Moreover, increased drug partitioning into the skin creating high drug concentration within the upper layers of the skin may result from the possibility that the formulation components can enter the skin as a monomer (158). In each system, all compositions can act as penetration enhancers with different mechanisms of action. Terpenes, volatile substances naturally found in essential oil, have been reported to possess good penetration enhancing abilities with low skin irritancy and low systemic toxicity (160-161). For hydrophilic compounds, the primary effect of terpenes as a penetration enhancer is to increase drug diffusivity in the horny layer which leads to the reduction of skin barrier properties (162). But for more lipophilic compounds, terpenes increase drug diffusivity and also increase drug partitioning into the stratum corneum (163). Surfactants have been reported to enhance the flux of materials permeating through biological membranes (103, 161). However, cationic and anionic surfactants which possess a pronounced effect have a potentiality to damage human skin (143). Triton X-114, a non-ionic surfactant, was therefore used in this study because of its safety and low chronic toxicity. Ethanol, which was used as a co-surfactant in this study, is commonly used in many transdermal formulations since it can exert its permeation enhancing activity through various mechanisms such as acting as a solvent to increase the solubility of the TD alkaloidal extract (143) and permeate into the stratum

corneum to alter the solubility properties of the tissue with a consequent improvement for the compounds partitioning into the membrane (144).

In our study, the liquid crystalline system shows the highest ability to enhance skin permeation of the TD alkaloidal extract. Microemulsions also show the skin permeation ability but in the less pronounced way. The results are in a good agreement with the previous study of Maghraby (2010) that both microemulsion and liquid crystalline preparations exhibited some enhancing transdermal delivery ability but he indicated the higher ability in enhancement of transdermal delivery of indomethacin in the microemulsion formulations than that of liquid crystalline preparations (158). Lopes *et al.* (2006) has also reported the enhancing ability of transdermal delivery of cyclosporine A from liquid crystalline systems comprising of monoolein and water (164) but the results were not compared with microemulsion. However, there are many studies that indicated the enhancing ability of microemulsions in transdermal drug delivery. Zhang and Michniak-Kohn (2011) has reported the increase of drug permeation flux and the cumulative permeation amount after 24 hr of the lipophilic drugs (ketoprofen and lidocaine) and a hydrophilic drug (caffeine) from microemulsions (152). Okur *et al*. (2011) has reported achieve percutaneous absorption rates of naproxen microemulsion (165).

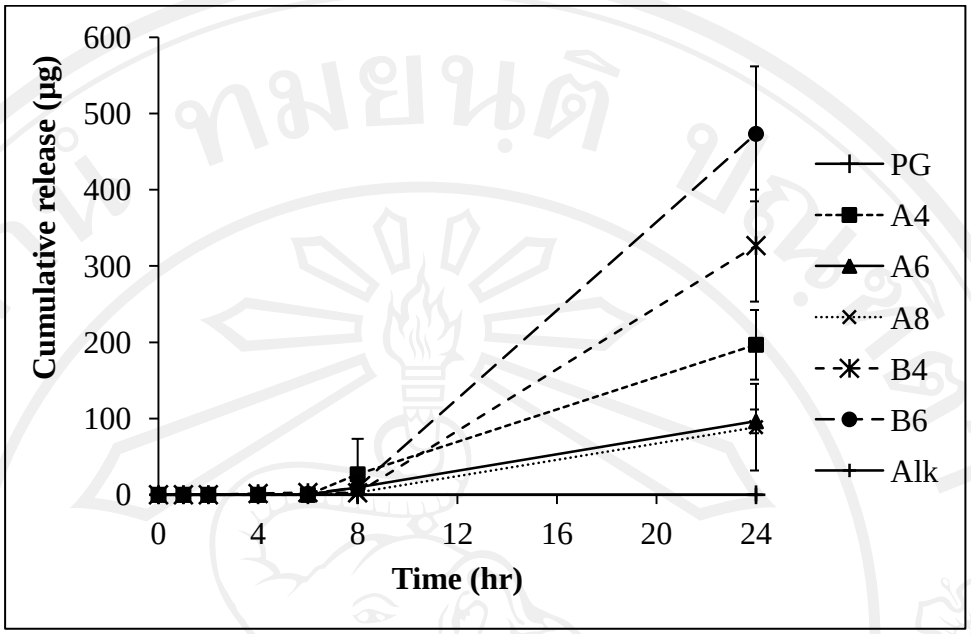

Figure 61 Cumulative release of TD alkaloidal extract (µg) versus time (hr) of PG (—+—), A4 (---■---), A6 (—▲—), A8 (····×····), B4 (-·✳·-), B6 (—●—) and the alkaloidal extract in PG (—+—).

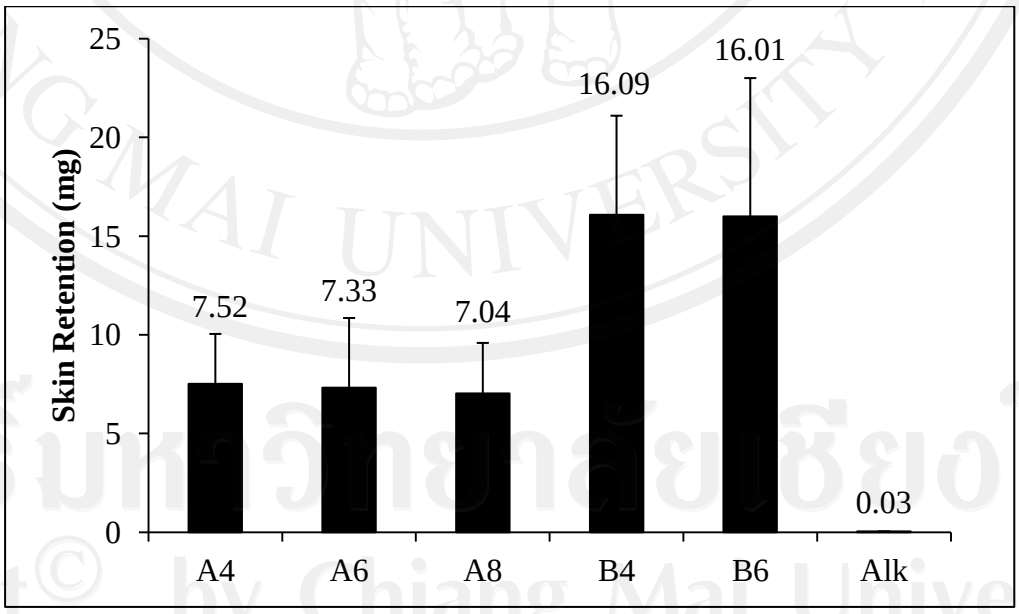

Figure 62 Skin retention of TD alkaloidal extract (mg) from each formulation 24 hr after application.